学位論文

Seasonal variation of the Tsushima Warm Current

(対馬暖流の季節変動)

Atsuhiko ISOBE (磯辺篤彦)

平成5年12月博士(理学)申請

東京大学理学系研究科
地球惑星物理学専攻

Seasonal variation of the Tsushima Warm Current

by Atsuhiko ISOBE

ABSTRACT

The volume transport of the Tsushima Warm Current in the Tsushima Strait has been believed to show a remarkable seasonal variation with variation range larger than 2 Sv, with its maximum value in summer-autumn and its minimum value in winter-spring. Such arguments, however, are based on geostrophic calculations assuming no current near the bottom or deduced from the seasonal variation on the sea level difference across the strait. Tawara et al. (1984) found that currents with significant magnitude exist near the bottom of the strait and indicated that the assumption of no current near the bottom would not always be valid. Recently, Egawa et al. (1993) indicated that the seasonal variation of the surface current of the Tsushima Warm Current is rather small by analyzing the data of Acoustic Doppler Current Profiler (ADCP). The purpose of this paper is to clarify the nature of the seasonal variation of the Tsushima Warm Current in the Tsushima Strait. The previous knowledge of the Tsushima Warm Current is shortly reviewed in Section 1.

In Section 2, results of the repeated ADCP and CTD observations are analyzed. The ADCP and CTD observations were made five times: on 4 July, 11 September and 31 October, 1990 and 4 March and 30 April, 1991. Total volume transport of the Tsushima Warm current deduced from the ADCP survey is about 1 Sv on 4 July 1990, on 4 March 1991, and on 30 April 1991, and is about 5 Sv on 11 September (the data is not available in the Western Channel on 31 October 1990, and was not used). If we have not the singular value on 11 September 1990, we may conclude that

there is no seasonal variation in transport. Since a snap-shot type of the measurement may be influenced by short-period fluctuations, and since the transport on 11 September appears to be reinforced by a strong wind, it is hard to conclude the nature of the seasonal variation from these limited data. It should be noted, however, that significant current velocity was observed near the bottom for all of these observations. This implies that the transport deduced by dynamic computation assuming no current near the bottom would be erroneous in the Tsushima Strait.

The CTD observations show that the bottom cold water, which originates from the Japan Sea Proper Water, exists in the Western Channel throughout the year. The ADCP observation in September shows a strong baroclinic current component just off the Korean coast in the Western Channel, being associated with the existence of the bottom cold water. Since such baroclinic current component produces no net volume transport, the knowledge of the seasonal variation of the bottom cold water is essential for estimating the seasonal variations of the current structure in the strait and of the sea level difference across the strait.

In Section 3, the influence of the bottom cold water on the current structure and the sea level distribution in the Tsushima Strait is investigated numerically by using a simple model of a baroclinic adjustment problem. We consider a channel with a rectangular cross-section. To describe the sharp seasonal thermocline, we adopted a five-layer system for summer condition, but a two-layer system for winter

condition where the stratification is very weak except the existence of the bottom cold water. The bottom cold water is treated as the lowest bottom layer, and a rectangular upheave of the upper boundary of the lowest layer is placed in still waters as an initial condition. By selecting suitable experimental parameters and the size and position of the upheaved portion so as that the resulted configuration of each interface and distribution of the current in each layer fit the observed ones, the surface current distribution and the sea surface distribution are estimated.

For the summer model (Model 1) in which the bottom cold water is placed just off the Korean coast in the five-layer system, the sea level at the Korean coast is lowered by about 8 cm relative to that at the Japanese coast. If we place the bottom cold water just off the Korean coast for the winter stratification (Model 2), the sea level drop at the Korean coast decreases to 3 cm. For the winter model in which the bottom cold water is shifted 50 km offshore for the winter stratification (Model 3), a sea level drop of about 1 cm occurs in midway of the strait and the sea level at the Korean coast is raised by about 2 cm, but the sea level at the Japanese coast is also raised by about 2 cm. So, the no sea level difference is resulted from the bottom cold water across whole strait in winter. When we confine our attention to the seasonal variation of the sea level across the Western Channel of the Tsushima Strait, the magnitude of the variation predicted by our model (difference between Model 1 and Model 3) reaches 11 cm, and is comparable with the observed value. This means

that the influence of the baroclinic motions induced by the bottom cold water on the sea level difference across the Western Channel is large enough to affect the estimation of the volume transport through the Western Channel from the observed sea level difference. It should be noted that the position of the bottom cold water plays an important role in producing a considerable sea level difference.

By combining the data of the sea level difference and of the hydrographic observations, we intend to estimate the seasonal variation of the net volume transport through the Tsushima Strait in Section 4. The data used in this section are the sea level data observed at Hakata, Izuhara and Pusan and the CTD data obtained by the Yamaguchi Prefectural Open-Sea Fisheries Experimental Station on monthly base during the period from 1988 to 1990. The vertical profile of the geostrophic current is calculated at each observation station, and the baroclinic component whose vertical integration is zero is obtained. Then, the baroclinic sea level difference resulted from the baroclinic current component was calculated across the Tsushima Strait for each observation time. The barotropic sea level difference, which is equivalent to the net volume transport through the Tsushima Strait can be estimated by subtracting the baroclinic sea level difference from the observed sea level difference. The results indicate that the total volume transport through the Tsushima Strait has a maximum in early winter and a minimum in early spring. The variation range of the volume transport is estimated to be about 0.7 Sv. This value is from

1/3 to 1/2 of the variation deduced only from the observed sea level difference where the effect of the baroclinic sea level difference is ignored.

CONTENTS

1. INTRODUCTION

The Japan Sea is connected to the adjacent seas through four straits: the Tsushima Strait to the East China Sea, the Tsugaru Strait to the North pacific and the Soya and the Mamiya Strait to the Okhotsk Sea. Subtropical waters flow into the Japan Sea through the Tsushima Strait to form the Tsushima Warm Current which is one of the major currents in the Japan Sea. The heat and salinity fluxes and the transport of larva through the Tsushima Strait are essential to the studies on the oceanography, meteorology and fishery science in the Japan Sea. Although the Tsushima Warm Current is strong and is well defined in the Tsushima Strait, its feeding current system in the East China Sea is obscure and no conspicuous currents can be observed in the sea west of Kyusyu. The Tsushima Warm Current Water consists of the mixed water between the Surface Kuroshio Water and the coastal shelf waters in the East China Sea (e.g., Lim 1971 and Nagata 1982). Because the sill depth of the Tsushima Strait is only about 140 m and because winter convection in this area easily reaches to the bottom, the Tsushima Warm Current has rather a shallow structure and its water characteristics exhibit a considerable seasonal variation.

The Tsushima Warm Current has been investigated by many oceanographers, and it has been believed that the transport or the current velocity of the Tsushima Warm Current in the Tsushima Strait shows a considerable seasonal variation. For example, Hidaka and Suzuki (1950) and Yi (1966) estimated the surface

current velocity of the Tsushima Warm Current in the Western Channel of the Tsushima Strait (see Fig. 1), and obtained values of about 80 $cm \cdot s^{-1}$ in August-October and of 20-30 $cm \cdot s^{-1}$ in December-May. However, since the direct current measurements are very few, the seasonal variation is usually deduced from the dynamic computation assuming that the current speed is negligible at the bottom, or from the seasonal variation of the sea level deference across the strait. Miita(1976) investigated current structure across the Strait in summer, using historical data of the direct current measurement in 1942 and 1943 where the measuring periods are 25 hours. They found that the intense current exists near the bottom of the Tsushima Strait, and shed the doubt about the validity of the dynamic calculation assuming zero velocity at the bottom.

The sea level difference across the Tsushima Strait is used as an indicator for the volume transport or the surface current velocity in the strait by many investigators (e.g., Kawabe, 1982 and Toba et al., 1982). As seen in Fig. 2, the sea level difference across the Western Channel of the Tsushima Strait shows significant seasonal variation, and the difference is large from August through October (maximum in August) and small December through May. This is another reason that the Tsushima Warm Current is thought to have a large seasonal variation.

Recently, Egawa et al. (1993) analyzed ADCP (Acoustic Doppler Current Profiler) data obtained on board the vessels belonging

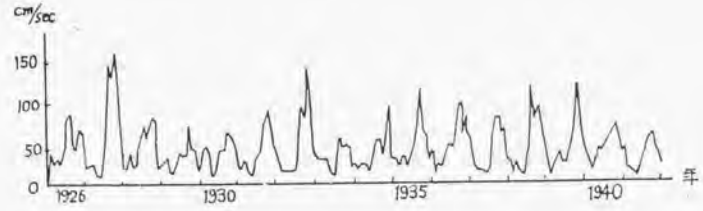

Fig.1. Temporal variation of the surface current velocity in the Western Channel of the Tsushima Strait, deduced from the dynamical computation assuming that the current speed is negligible near the bottom. (after Hidaka and Suzuki, 1950).

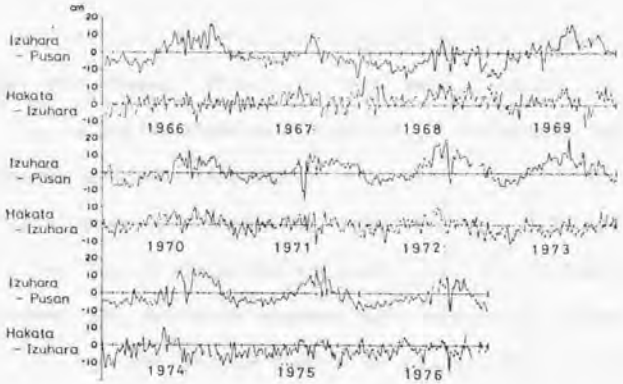

Fig.2. 5-day running means of difference in daily mean sea level between Izuhara and Pusan and between Hakata and Izuhara from 1966 to 1976. The mean value of each curve fro the whole eleven-year period is taken as the zero point of the ordibate. The difference are obtained by subtracting the value at Pusan from those at Izuhara, and the value at Izuhara from those at Hakata. (after Kawabe, 1982)

to the Maritime Safety Agency during the period from February 1987 to November 1990. As the main source of the data is patrol boats, the data are available for all months in the area of the Tsushima Strait. They pointed out that the seasonal variation of the currents in the strait is much smaller than that suggested in the previous papers, and that the northeastward current component of the main flow in the Western Channel is relatively high October through December.

The main part of the Tsushima Warm Current flows out into the Pacific Ocean through the Tsugaru Strait. It has been also believed that the transport through the strait shows a large seasonal variation. However, the results of the direct current measurements using bottom installed ADCP (Shikama et al., 1991) indicate that the seasonal variation of the transport through the Tsugaru Strait is very small, though the stratification and the water mass properties of the current show considerable seasonal variations.

In this study, to clarify the reason of the discrepancy between the past knowledge and the recent observational results and to know the details of seasonal variations of the oceanic conditions in the Tsushima Strait, the data of the repeated ADCP surveys across the Tsushima Strait will be analyzed along with CTD data. It will be shown both through data analysis and simple numerical experiment that the sea level difference across the strait is largely influenced by baroclinic motions which produce no net volume transport. It will be also discussed how we can estimate the seasonal variation of the net volume transport

from the sea level difference data by removing the effect of baroclinic motions.

2. *CURRENT STRUCTURE IN THE TSUSHIMA STRAIT AND ITS VARIABILITY DEDUCED FROM REPEATED ADCP AND CTD OBSERVATIONS IN 1990-1991*

2.1 OBSERVATIONS

ADCP(belonging to Research Institute for Applied Mechanics of Kyushu University) observations across the Tsushima Strait were repeatedly carried out on board the R/V Kuroshio-Maru of the Yamaguchi Prefectural Open-Sea Fisheries Experimental Station in 1990-1991. The observation line (see Fig. 3) is a part of the routine observation network of the experimental station. CTD measurements were carried out at Stations 1 through 9, but the order of occupation is different for each observation run. The ADCP measurements were made between all of these CTD stations. The observation was carried out five times during the period; 4 July, 11 September and 31 October, 1990 and 4 March and 30 April, 1991. The starting time of the CTD measurement at each station for each observation run is listed in Table 1. The edge of the line (Station 1) on the Japanese side is located just off Kawajiri-misaki, but on the Korean side (Station 9) is selected to be about 30 km offshore of Ulsan, just outside the Korean territorial water.

The towed-type of ADCP system developed by Kaneko et al.(1990) was used. The fish of the ADCP was towed by 50 m long rope, and adjusted to be at 8 m depth during the measurement. The signal is sent to the recorder on board. The Tsushima Strait is shallow enough to use a return signal from seabed to determine the

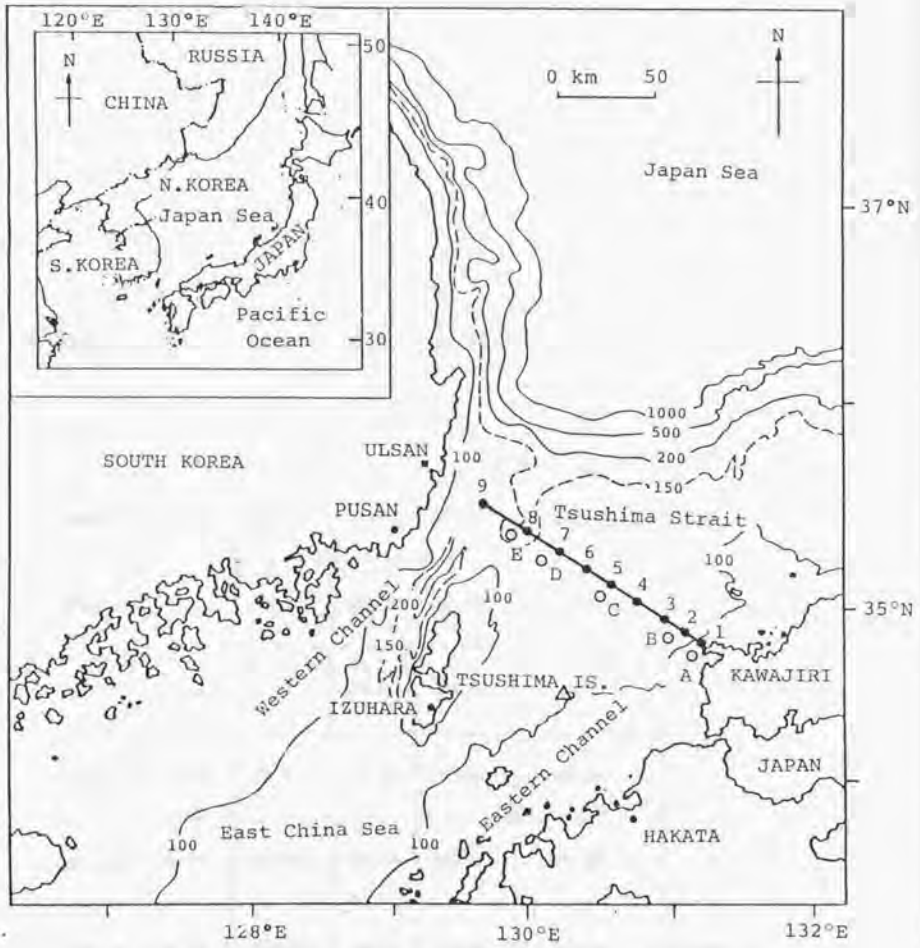

Fig.3. The bathymetric chart in the vicinity of the Tsushima Strait. The numerals attached to the isobath indicate the depth in m. ADCP observation line is shown with bold strait line, and the the positions of the CTD observations, Sta. 1 through Sta. 9 are shown in black circles. Open circles show the positions of tidal current observations conducted by the Imperial Navy in 1942 and 1943. A open triangle in the eastern channel denotes the position of the tidal current observation, the data of which was analyzed by Odamaki (1989). This point is used as a reference point in this study.

Table 1 Time table for ADCP surveys

	1990			1991		
	4 July	11 Sept.	31 Oct.	4-5 Mar.	30 Apr.~1 May	
Sta.1	04:02	19:01	12:01	15:42	12:47	Japan
Sta.2	06:25	18:03	12:57	16:46	13:53	
Sta.3	07:50	16:34	14:15	18:02	15:12	
Sta.4	09:20	15:07	15:35	19:23	16:30	
Sta.5	10:40	13:40	16:50	20:46	17:50	
Sta.6	12:00	12:17	18:09	22:02	19:09	
Sta.7	13:30	10:59	19:23	23:24	20:26	
Sta.8	14:50	09:40	20:40	00:55	21:45	
Sta.9	16:52	07:15	22:43	03:00	00:56	Korea

movement of the ship, and the current profiles relative to the seabed were obtained (e.g., Simpson et al., 1990). Velocity data were sampled every minute at depth intervals of 8 m. When the irregular fish motion occurs accidentally and the rolling and pitching angles vary considerably, the ADCP signals become erroneous. By checking the signals on fish motion, we eliminated such erroneous data. Due to the acoustic shadow zone, ADCP data are not available in the bottom layer, the thickness of which is about 14 % of the total depth (Kaneko et al.,1988), and the extrapolation procedure is needed to obtain the volume transport.

2.2 TIDAL CURRENT CORRECTION

There exist strong tidal currents in the Tsushima Strait, and its magnitude exceeds one knot in the western channel of the Tsushima Strait (Odamaki, 1989). To obtain the net transport through the strait, we need to subtract tidal components from the ADCP velocity data.

The direct measurements of the tidal current components were carried out near our observation line in 1942-1943, and the data are available in the JODC catalog (JODC, 1985). The position of the observations are shown in Fig. 3 with open circles: Stations A through E. The data lengths of these observations are one lunar day, and only the harmonic constants of the diurnal tide M1, the semi-diurnal tide M2 and their higher constituents such as M4 component having about 6 hours period would be

calculated. As these harmonic constants vary with lunar age and declination of the moon on the observation day, these data cannot be used for our tidal current correction, directly. The more complete tidal data are available at the sites shown with a open triangle in Fig. 3, and Odamaki (1989) gave the harmonic constants of the "Principal lunar" M_2, "Principal solar" S_2, "Luni -solar diurnal" K_1 and "Principal lunar diurnal" O_1 tidal current constituents for this point. Yanagi and Higuchi (1980) gave a method to convert the data of M1, M2, and M4 constituents into the harmonic constants of the M_2, S_2, K_1 and O_1, when there are accurate data on these constituents at some reference point nearby. The tidal currents in the strait are predominant in the direction parallel to the axis of the strait, and the basic nature of the tide at Odamaki's point is considered to be the same as those at Stations A through E. By choosing Odamaki's point as a reference point, we calculated the tidal current velocities at Stations A through E at the time of ADCP observations.

By using the harmonic constants of the four principal components, M_2,S_2,K_1 and O_1 given by Odamaki (1989), the tidal current at the reference point was calculated for the day of each current measurement, and the harmonic constants for M1 and M2 constituents was calculated at the reference point. Using the harmonic constants for M1 and M2 constituents, we calculated the ratios of the amplitudes at each station to those at reference point, the difference between the phase lags at each station and those at reference point. The harmonic constants of M1 and M2

components at each station were converted to those of the four principal components by using the calculated ratios and differences. In this procedure, the ratios and the differences for K_1 and O_1 and for M_2 and S_2 are assumed to be the same.

By using these constants, the tidal current at Stations A through E at the time of ADCP measurements were calculated as shown in Fig. 4. Tidal currents along the ADCP observation line were obtained by linear interpolation from estimated values at these stations which are assumed to be aligned on the line. For the portion between Stations 8 and 9, northwest of Station E (Station 8), the current were interpolated by assuming the current at the Korean coast is zero. We considered only the barotropic tides, and the influence of the internal tides are ignored.

2.3 RESULTS OF THE OBSERVATION

2.3.1 Hydrographic observations

The obtained cross-sectional distributions of temperature, salinity and sigma-t are shown in Figs. 5, 6, and 7, respectively. In each figure, the distributions for five observational runs are shown in (a) through (e).

As seen in the distributions in September 1990 (Fig 5b, 6b and 7b), the sharp thermocline and halocline develop in the summer. The stratification is also clearly found in July 1990 and in October 1990, and a warm and less saline water occupies the upper layer to form a sharp pycnocline below it. The

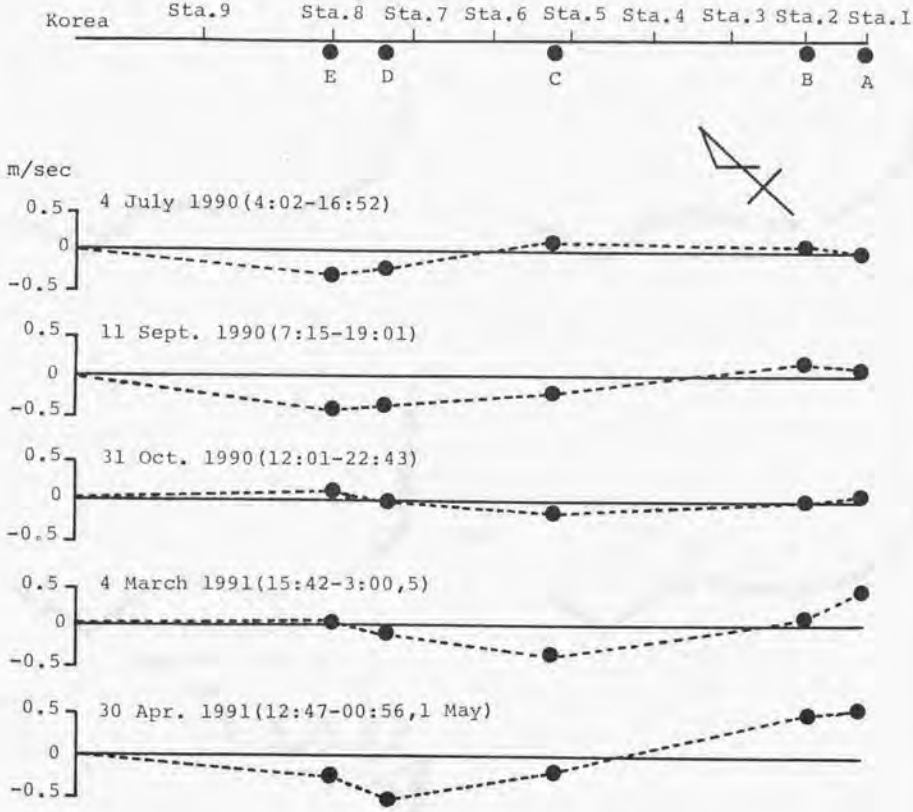

Fig.4. Distribution of the northeastward component of the predicted tidal current at each time of the ADCP observation. The uppermost figure shows the position, where the tidal current component is predicted, relative to the ADCP observation line. The attached Sta. numbers indicate the positions of the CTD observations. The positions are located very near to the line, and we assumed that the positions are aligned on the line. The dates attached to the each figure indicate the starting time and terminating time of the coverage of the ADCP observation line. The northeastward current is taken to be positive.

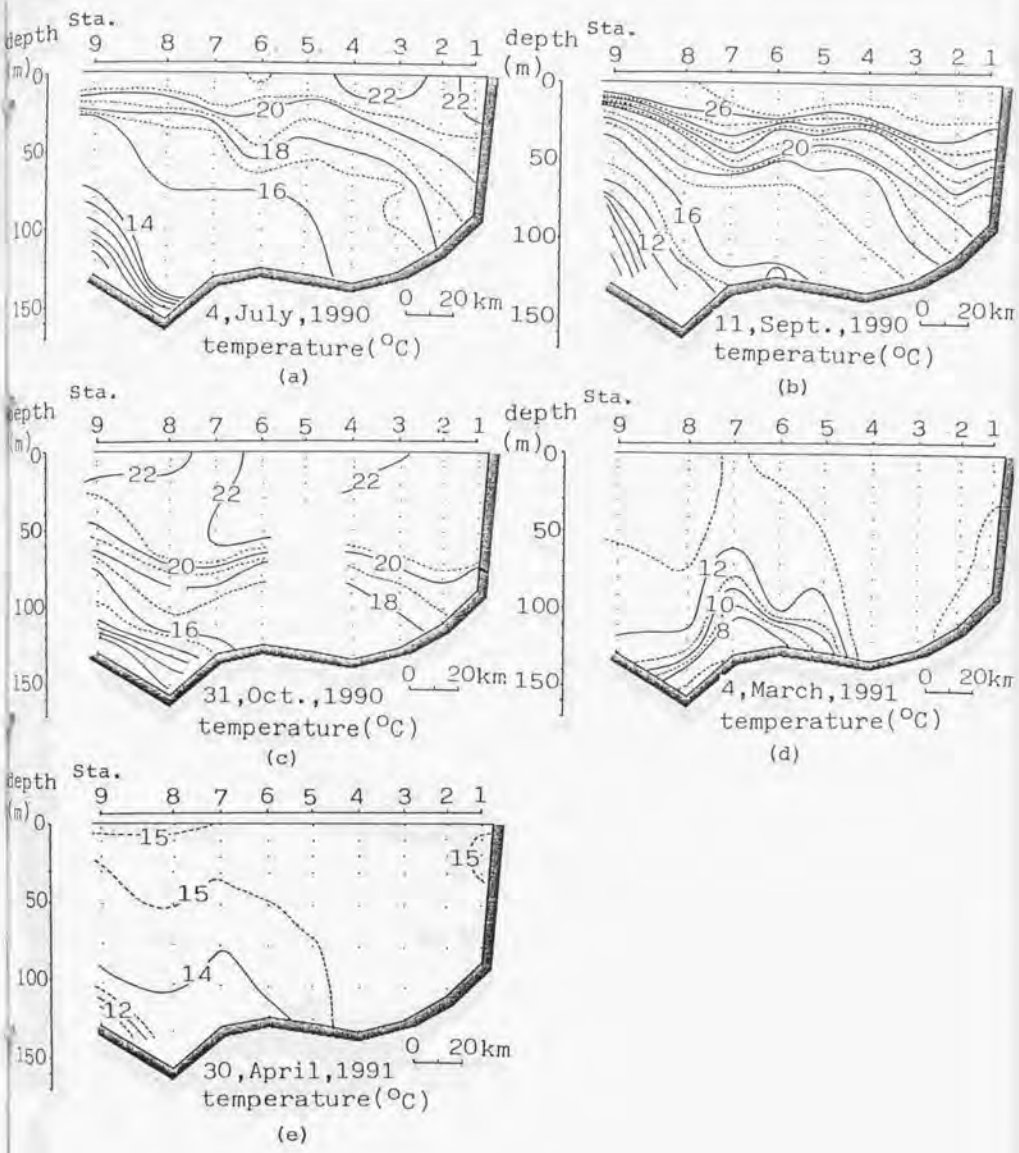

Fig.5. Coss-sectional distributions of water temperature in °C. The depth in m is taken in the ordinate, and the scale of the horizontal axis is shown in the right-bottom of each figure. The positions of the CTD stations are shown above each figure. The date of the observation is shown below each figure(a-e).

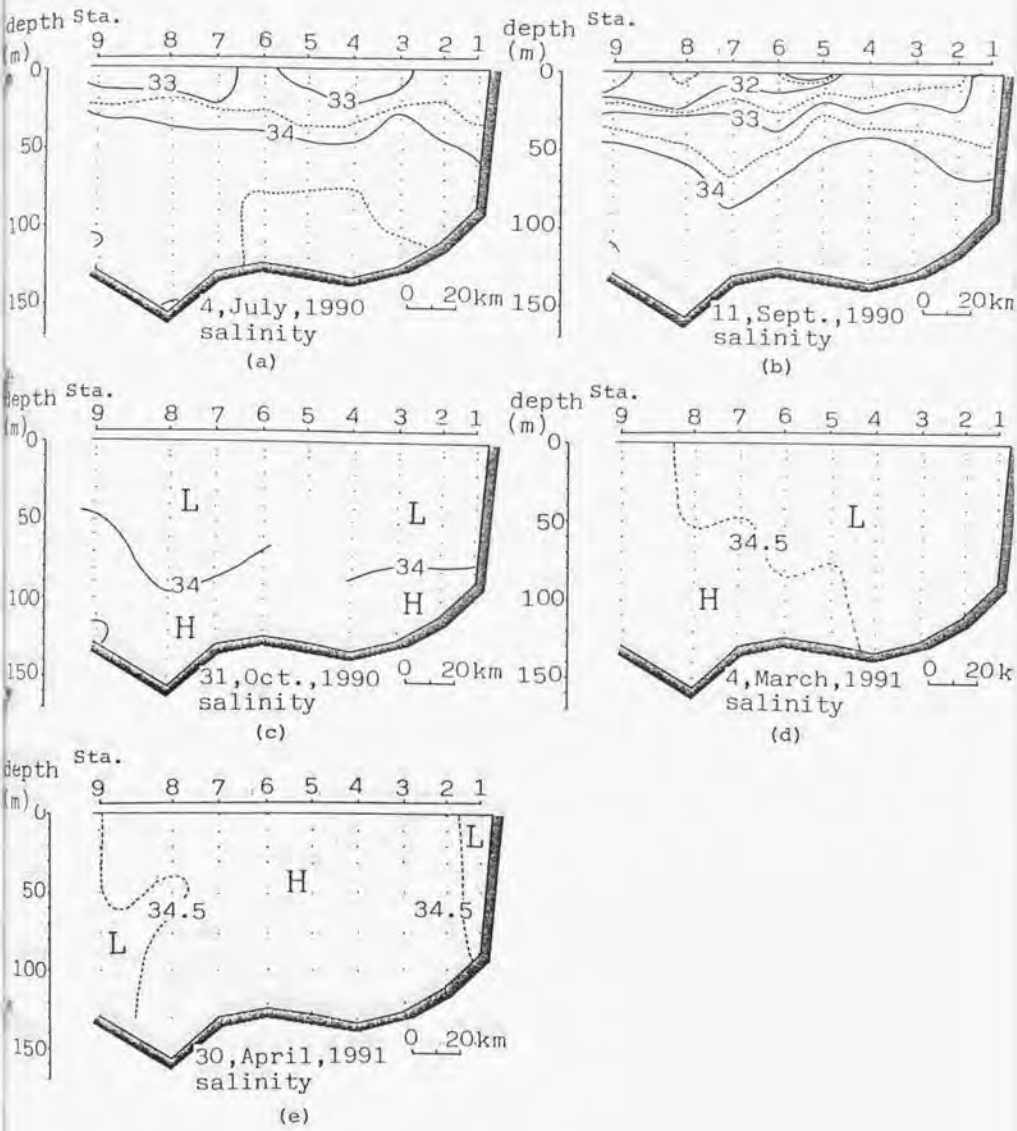

Fig.6. Cross-sectional distributions of salinity.

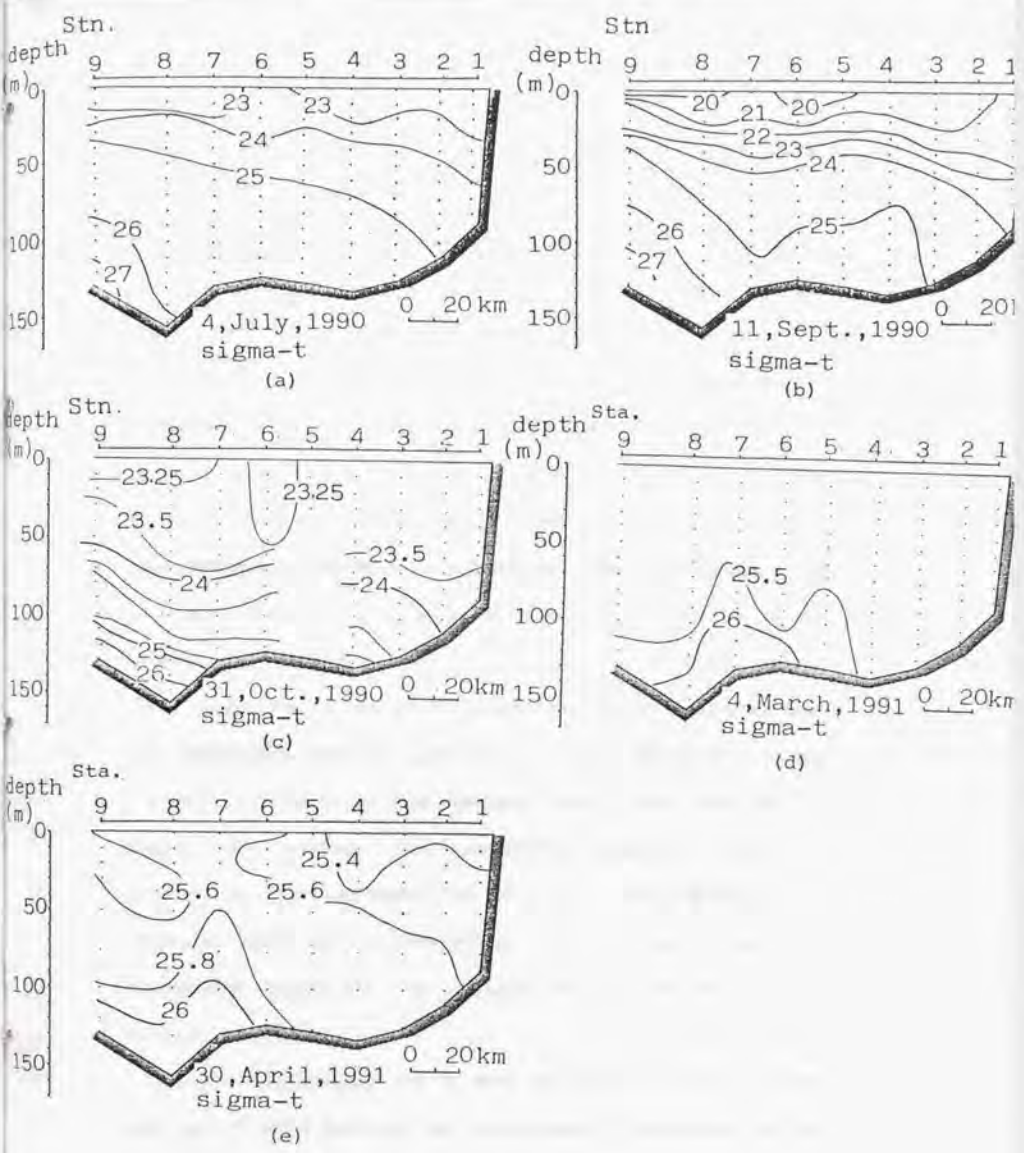

Fig.7. Cross-sectional distributions of sigma-t.

thickness of the layer increases in October. On the other hand, the stratification is very weak in March 1991 and in April 1991, indicating that the winter convection reaches nearly to the bottom. However, near the bottom from Stations 5 to 9, some stratifications in temperature and sigma-t are found, and will be discussed later.

As typically shown in the distribution in July, some wiggle of isotherms (also in isopycnals) or S-shaped structure can be observed near Station 6. By analyzing 15-year hydrographic data in this region, Ogawa(1983) showed that the S-shaped configuration of the seasonal pycnocline in the cross-section is a common feature in this region. This structure is often assessed as an eddy formed on the lee side of Tsushima Island (e.g.,Isoda,1989), but, at least partly, can be accounted for the adjustment process associated with the intrusion of the bottom cold water in the Western Channel (see Section 3). Except this portion, the isopycnals generally tend to slope down southeastward (to the right in the figures). This suggests that the northeastward currents (at least, the geostrophic component) are dominant both in the western and eastern channels.

Another thermocline can be found in deeper depths between Stations 8 and 9 just off the Korean coast. This thermocline is observed throughout the year. Kawabe (1982) discussed on the vertical distribution of the sigma-t in this region in 1973, and pointed out that the thermocline corresponding to this deeper thermocline is a continuation of the main thermocline found in

the Japan Sea. This thermocline always accompanies a strong pycnocline. Hereafter, we shall refer this thermocline as the main thermocline.

The main thermocline is formed above a cold water existing near the bottom just near Korean coast. The thermocline is sharp in summer (in July and in September), but the temperature at the center of the cold water appears not to change considerably. Kawabe(1982) and Ogawa (1983) also indicated the existence of the main thermocline or pycnocline and its seasonal variations which is the same as we observed. In the temperature distribution in September, the depth of the main thermocline appears to decrease in comparison with other months. Though it is hard to conclude from our limited data, this might be related to the cold water upwelling near the Korean coast in summer (Byun, 1989). A very fresh water having the salinity less than 32 psu is found in the upper layer of the western channel in September. The appearance of the fresh water in summer was reported by various investigations (Uda,1934; Uda,1936; Kajiura et al.,1958; Kawabe,1982; Ogawa,1983).

2.3.2 ADCP surveys

The horizontal velocity field obtained by ADCP measurements is shown in Fig. 8 with stick diagram for each observation run. The horizontal velocities shown here are raw data without tidal correction. The upward component of the vectors denotes the northward velocity, and the rightward component the eastward velocity. The maximum velocity measured was about 80

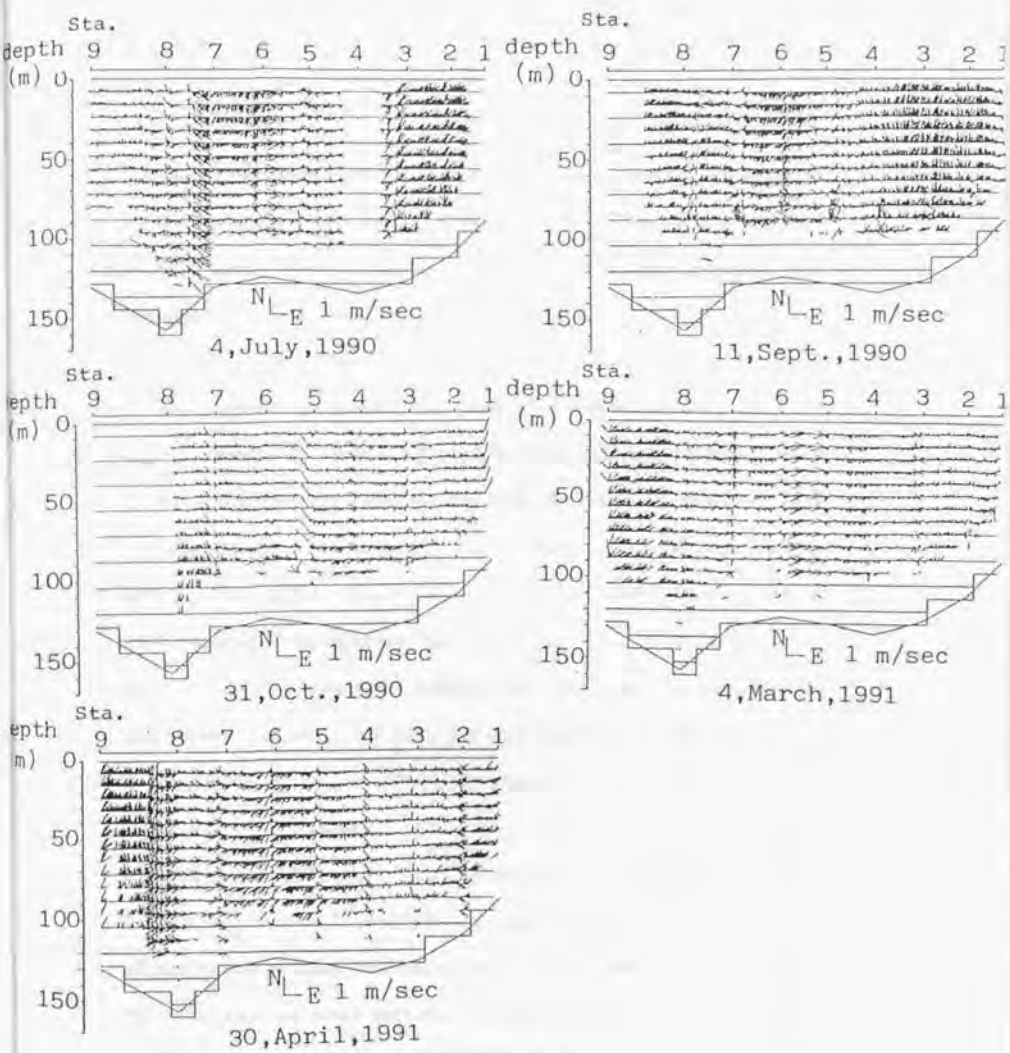

Fig. 8. Horizontal velocity field obtained by ADCP observations. The velocities are shown in vectors by taking the northward component upward, and the east component rightward. The magnitude of the vector is shown at the bottom of each figure. The tidal current correction has not been made. The date of the observation is shown below in each figure.

$cm \cdot sec^{-1}$, while the predicted tidal components are less than 50 $cm \cdot sec^{-1}$ during these observations (see Fig. 4).

The northward or northeastward currents prevail except in the central part near Station 6. In the central part, weak southward or southwestward currents appear to exist, though some of them may be induced by tidal currents. The gross current feature shows good correspondence to the results of the hydrographic observations discussed in the previous sub-section. Since we need about 12 hours for each observation run, the tidal components would vary gradually across the section. The short wave variations of the obtained current fields would result from current fluctuations both in time and space or from internal tide components. We made tidal current corrections by using the method described previously, and then removed small-scaled fluctuations by smoothing the data with a 10 km x 16 m rectangular window. The resulting current fields are shown in Fig. 9 for the northeastward component. The northeast direction roughly corresponds to the direction of the axis of the strait, and are perpendicular to the section. In figures, the northeastward component is taken to be positive as it corresponds to the main current direction of the Tsushima Warm Current in the strait. Hereafter, we shall call the southwestward current component as a countercurrent.

The maximum velocity always takes place in the Western Channel (to the northwest of Station 7), except in October, 1990 when no data available there. The maximum velocity is found in the September section, and exceeds 80 $cm \cdot sec^{-1}$. The current in

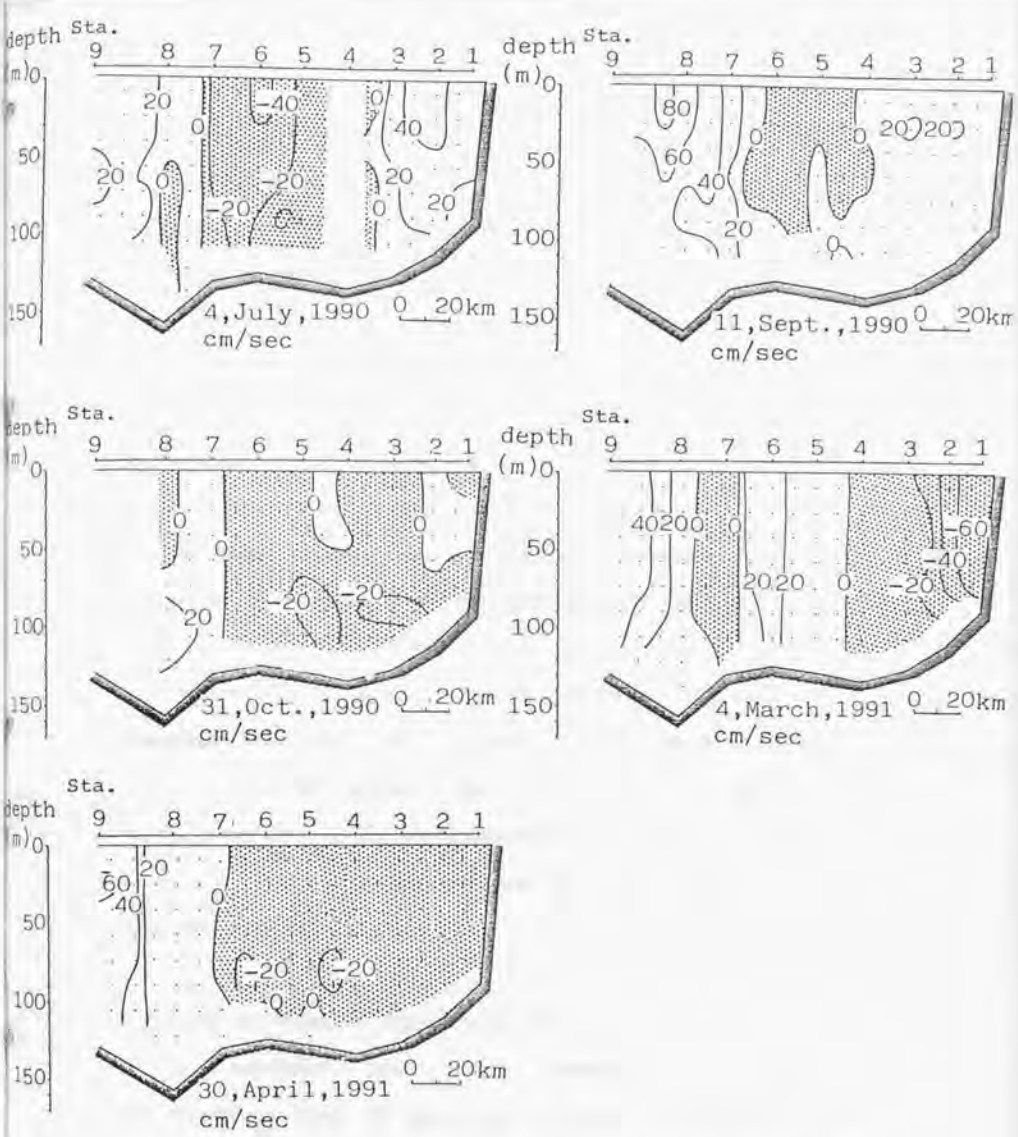

Fig.9. Distributions of the northeastward component of the current velocity in cm/sec. The northeastward direction is perpendicular to the section and coincides roughly with the strait axis. The tidal correction (see Section 2-2) has been made, and the values are smoothed by taking average for each 16m x 10 km rectangular area. The date of the observation is shown below each figure. The domains where the current is southwestward are shaded.

the western channel is barotropic except in September, 1990 when the stratification is most significant (see Fig. 7(b)). The current field in the eastern channel is much more variable, and a northeastward current zone is seen near the Japanese coast only in the July and September sections, but the current direction is rather southeastward in the other sections. The maximum value is found in the July section, and is about 40 $cm \cdot sec^{-1}$. The magnitudes of the velocity obtained in the western and eastern channels are very similar to those given by Miita (1976) for summer season.

The countercurrent appears in all sections shown in Fig. 9, but its width and strength are variable section by section; it is very strong in the July section and is concentrated within a limited narrow zone of the central part in the July and September sections, but spreads out for whole eastern channel in the October and April sections. In the March section, the countercurrent is separated into two zones; one is in the central part and the other is located just near the Japanese coast.

2.3.3 Volume transport deduced from ADCP data

To calculate the volume transport (vertically integrated velocity) at each point, we need to estimate the current velocity fields in the bottom shadow zone where no ADCP data are available. We applied three different methods. In Case 1, we assume no current in the shadow zone. In Case 2, the velocity is assumed to vanish at the bottom, and the velocity

profile in the shadow zone is linearly interpolated. The more elaborate method is adopted in Case 3, and the velocity profile in the zone is extrapolated in quadratic form as follows (Bowden and Fairbrain,1952):

$$u(\xi)=\bar{u}\cdot(1.15-0.425\cdot\xi^2) \qquad (2\text{-}1)$$

where $\bar{u}$ is the vertically averaged velocity in the upper layer where ADCP data exist, ξ is the fractional depth defined by the ratio z/h of the depth z to the total depth h. This profile is applied to the shadow zone.

We have no data between Station 9 and the Korean coast. The volume transport in this region is assumed to decrease from the value at Station 9 to zero at the Korean coast. In the case of September, the data near Station 9 were missing, and the station nearest to Korea is used instead of Station 9. In the case of October 1990, the data were missing in the broad area in the western channel, so we did not estimate the volume transport there. If the data gap exists in the velocity data along the observation line, the velocity there is given by linear interpolation from the velocity profiles at nearby two ADCP stations where data exists.

The volume transports are calculated at intervals of 10 km along the observation line for each run, and shown in Fig. 10 for three cases of the extrapolation on velocity profile in the shadow zone. The northeastward volume transport is taken upward. The results for three cases of extrapolation are almost

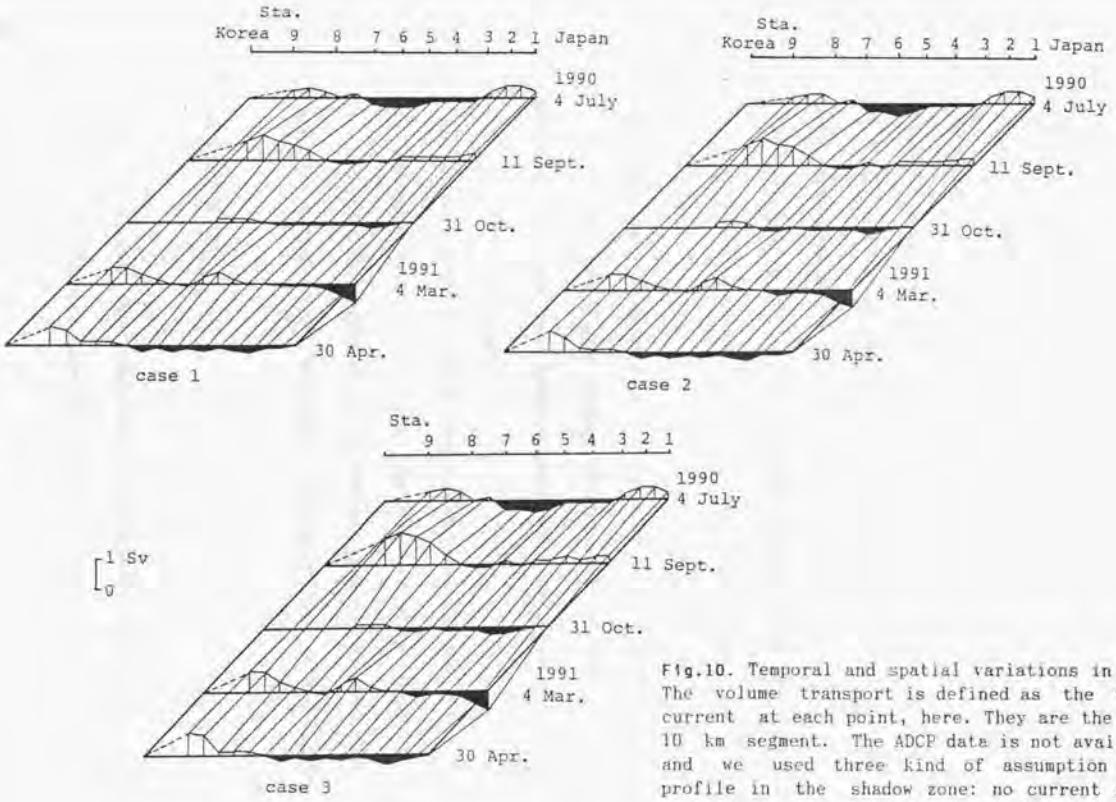

Fig.10. Temporal and spatial variations in the volume transport. The volume transport is defined as the vertically integrated current at each point, here. They are the total values for each 10 km segment. The ADCP data is not available near the bottom, and we used three kind of assumption to fill the current profile in the shadow zone: no current in the shadow zone is assumed in case 1 (the upper left figure), a linear profile vanishing at the bottom in case 2 (the upper right figure), and a quadratic profile in case 3 (the lower figure). See the text for details. The shaded region indicates southward volume transport.

identical, and the contribution from the shadow zone appears to be small.

It can be clearly seen also in these figures that the northeastward volume transport is large in the western channel for all sections. In the eastern channel, the northeastward transport appears in July, whilst the southwestward transport is dominant in March. The volume transport is small in September, October and April. A relatively strong northeastward current is observed along the Japanese coast in the July and September sections, but a southwestward current appears in the October, March and April sections.

By integrating the volume transport shown in Fig. 10 across the strait, the total transport through the Tsushima Strait is obtained for each observation run, and shown in Fig. 11. As the ADCP data are not available for the wide area in the western channel and the strong current zone appears to exist in that area in the case of October 1990, we do not calculate total transport for this case.

The total transport through the strait shows the maximum value in September, and is 4.0-5.9 Sv, the value of which depends on the extrapolation method of the current profile in the shadow zone. The transport for the other observation runs is 0.7-1.0 Sv.

2.4 DISCUSSIONS

The repeated ADCP observation indicates that the total transport through the Tsushima Strait is very large in September,

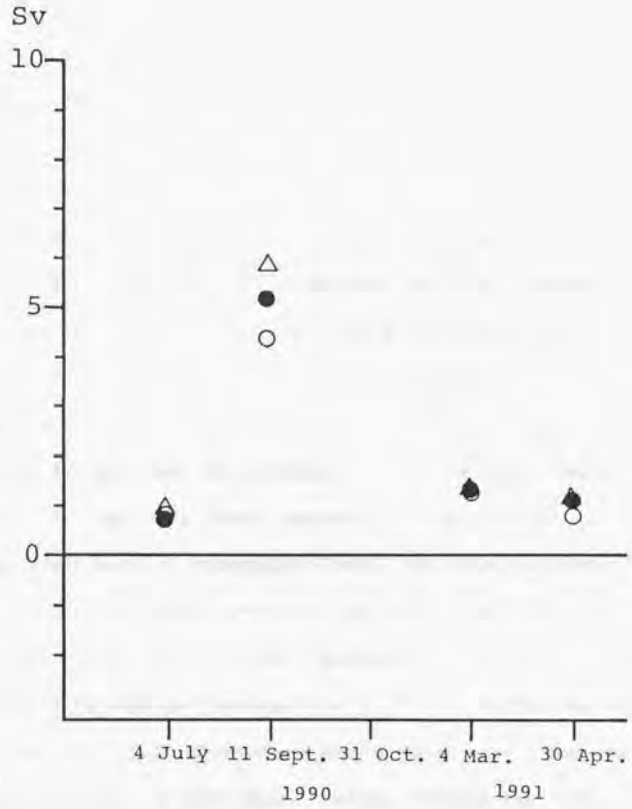

Fig.11. The total volume transports in Sv (the integrated transport over the whole section) for four observation times. The integration does not made for the data on October 31, as the data are not available in the Western Channel where the strong current zone of the Tsushima Warm Current flows. Open circles denote the estimations for Case 1, and the closed circles for Case 2, the open triangles for the Case 3.

1990, and is about 5 Sv. This might support the results of the previous studies (Hidaka and Suzuki,1950;Yi,1966). The transport estimated in July 1990, in March and April 1991, however, has almost the same value of order of 1 Sv, and this suggests that the seasonal variation is small or, at least, is not sinusoidal. If we have not a singular value in September, we might conclude that there is very small seasonal variation.

It should be noted that the transport estimated from ADCP data is of a type of snapshot, and that the value may be affected by fluctuations having shorter periods. The total transport in September might include temporary wind drift transport, as strong southerly winds of 7 in Beaufort's wind-force scale were observed during the observation (see Fig. 12). This may happen to increase the transport value in the observation time. In addition, tidal current correction used in this paper might have a systematic error. The effective number of our observation runs is only 4, and is too small to get any concrete conclusion on the seasonal variation of the transport through the Tsushima Strait. It is highly desired to increase the ADCP observations and to cover the observation line regularly. In this paper, further discussions for the seasonal variation of the total transport will be made by analyzing the hydrographic data together with the data of the sea level difference across the strait in the following sections. One of the interesting features in the cross-sectional current distributions in Fig. 9 is the barotropic nature of the current

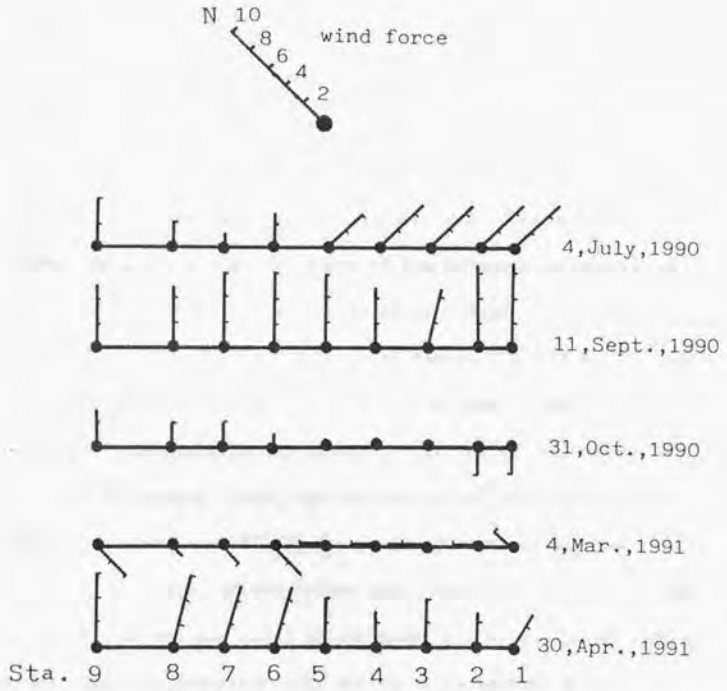

Fig.12. Wind in the Beaufort's scale measured on the ship during observations

structure. The significant current velocity is observed near the bottom throughout a year. This implies that the transport deduced by dynamic computation assuming no current near the bottom would be erroneous in the Tsushima Strait and gives an underestimate of the transport value. Miita (1976) reported that the northeastward current is intensified in the upper layer of the Western Channel in summer. This phenomenon is clearly seen in the current structure in September 1990 (Fig. 9). The another complexity of the oceanic structure of the Western Channel is the existence of the main thermocline near the bottom. The main thermocline gives a upper boundary of the bottom cold water, and the bottom cold water appears to originate from the upper part of the Japan Sea Proper Water or the thermocline water in the Japan Sea (Byun and Seung, 1984 and Lim and Chang, 1969). The water temperature at the center of the water is relatively constant throughout year, but its thickness and the position appear to make significant seasonal variation as seen in Fig. 5. The variation of the bottom cold water would cause the variation of the sea level height along the Korean coast. This effect will be quantitatively estimated in Section 3.

To see the baroclinic nature of the current structure and its seasonal variation, baroclinic components of the northeastward current are calculated at each observation point by subtracting the vertically averaged velocity from the velocity shown in Fig. 9. The results are shown in Figs. 13(a) and (b) for the cases of September, 1990 and March, 1991, respectively. The former would represent the summer state with strong

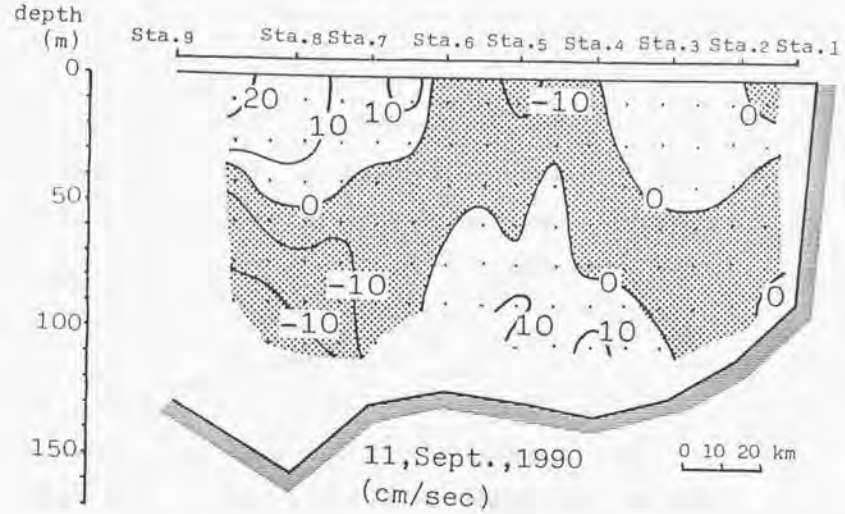

(a)

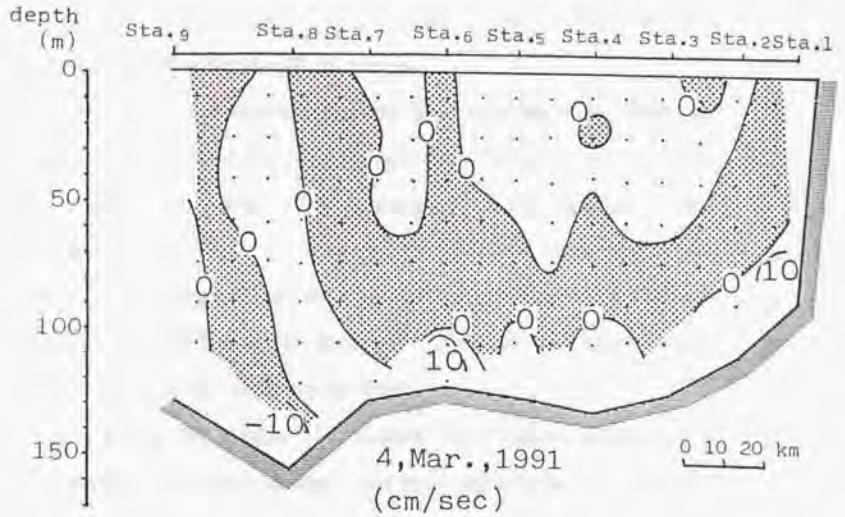

(b)

Fig.13. The same as in Fig. 9, except for the northeastward component of the baroclinic flow in cm/sec: (a) in September 1990 and (b) in March 1991. The former is conseidered as a representative for summer-autumn contdition, and the latter for winter-spring. The shaded area indicates southwestward flow.

stratification and the latter the winter state with weak stratification. The northeastward component is taken to be positive. It can be clearly seen that the baroclinicity or vertical current shear is strong in summer and weak in winter according to the strength of the stratification. In summer, the strongest vertical shear is seen just off the Korean coast in the western channel. The difference of the current speed between at the surface and at the bottom exceed 30 $cm \cdot sec^{-1}$. As seen in Fig. 5(b), the first thermocline (the seasonal thermocline) is located at about 30 m depth and is the most sharp in the cross-section. Also in this region, the clear main thermocline exists in the depth range from 50 to 100m above the bottom cold water. This strong shear zone seems to be created by the intensified surface current (Tawara et al., 1984) and the bottom cold water developed in summer.

In winter, the current shear is generally small as seen in Fig. 13(b). However, a significant baroclinic velocity with magnitude larger than 10 $cm \cdot sec^{-1}$ can be seen near the bottom at Stations 1, 6 and 8. It should be noted that the bottom cold water exists near the bottom around Stations 6 and 8 (see Fig. 5(d)), and the baroclinic currents seen there would be related to the bottom cold water.

As discussed above, the bottom cold water exhibits a considerable seasonal change, and this influences the current nature in the Western Channel where the main part of the Tsushima Warm Current flows through. To see the effect of the seasonal variation of the bottom cold water on the current field

and on the sea level height, we shall deploy simple numerical experiments in the next section.

3. THE BOTTOM COLD WATER AND ITS INFLUENCE ON SEA LEVEL DISTRIBUTION IN THE TSUSHIMA STRAIT

3.1 THE BOTTOM COLD WATER IN THE WESTERN CHANNEL OF THE TSUSHIMA STRAIT

As discussed in the previous section, it is reported that the bottom cold water is observed in the Western Channel for all of our five observation runs, and it is suggested that the variation of the nature of the bottom cold water influences strongly on the current structure in the Western Channel where the main part of the Tsushima Warm Current flows through.

The horizontal distribution on the level just above the bottom in the Western Channel of the Tsushima Strait in August 1963 and in November 1966 are cited in Fig.14 from Lim and Chang (1969). They argued that the origin of the bottom cold water is the Japan Sea Proper Water on the basis of hydrographic data analysis. Byun and Seung (1984) confirmed this argument by their direct current measurement.

To check whether the cold water found in September 1990 in our observation is the bottom cold water or not, we draw the horizontal temperature distribution just above the bottom in the western channel in August 1990 by using the data obtained by the National Fisheries Research and Developed Agency of Korea (NFRDA, 1992) (Unfortunately, no observation was made in September 1990). The result is shown in Fig. 15. It can be seen that the bottom cold water is clearly extended from the Japan Sea into our

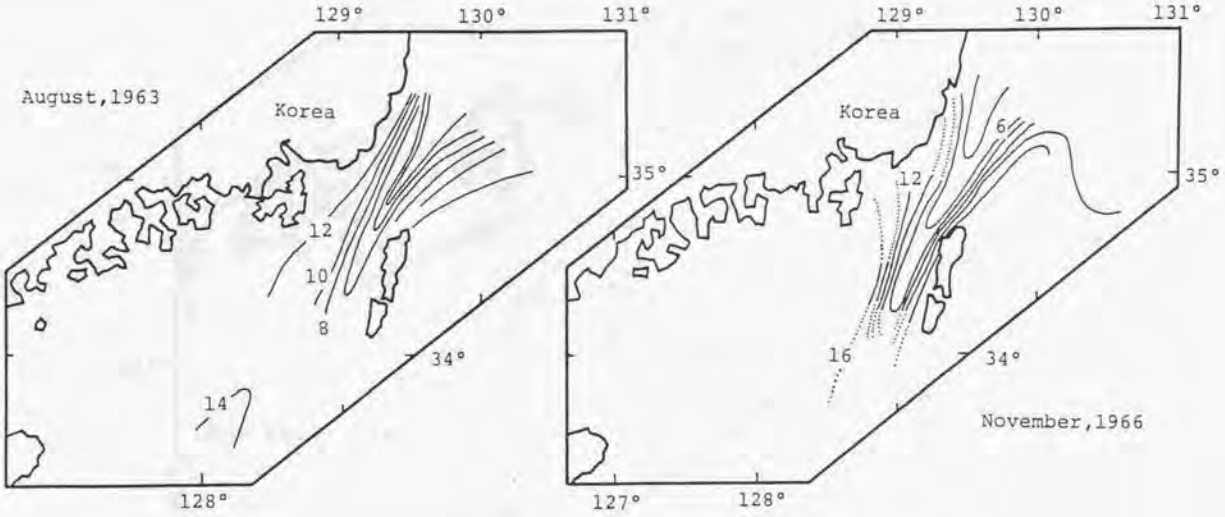

Fig.14. Horizontal distributions of the temperature in °C in the bottom layer of the Western Channel in August 1963 (the left figure) and in November 1966 (the right figure). (after Lim and Chang,1969)

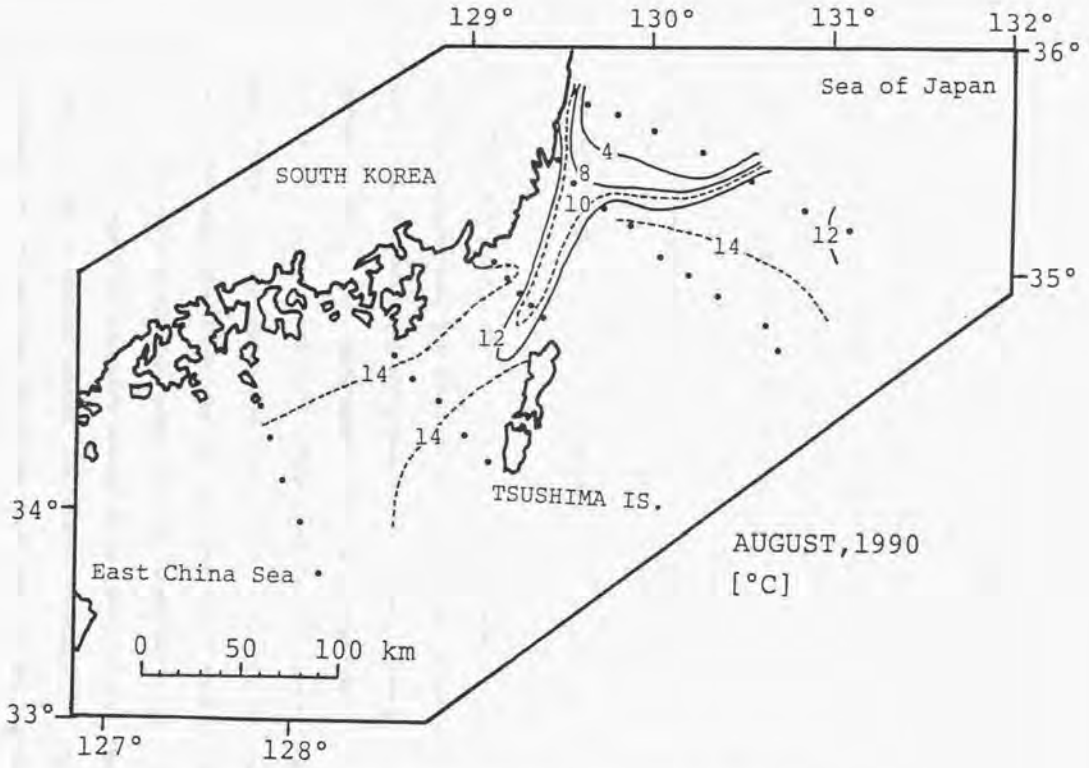

Fig.15. Horizontal distribution of the temperature in the bottom layer of the Western Channel in August 1990.

observation site in the summer of 1990.

In this section, the influence of the bottom cold water on the sea level distribution in the Tsushima Strait will be investigated by a simple numerical model experiment of baroclinic adjustment. Namely, we shall put the bottom cold water in a layered strait with no motion, and watch the time variation of the currents and the depth(s) of the interface(s). By adjusting the initial conditions, we seek the distribution of the sea level across the strait when the induced current and stratification almost fit to the observed states.

3.2 MODEL USED AND NUMERICAL PROCEDURE

The southwest edge of the bottom cold water is usually located near the southern tip of Tsushima Islands, and has a three dimensional structure. In this study, however, we assume that the phenomenon can be described two dimensionally for simplicity. This simplification may not be applicable to the region near the southwestern tip of the cold water area, but it position is far from our observation site. The scale of the cold water in the direction along the strait axis would be reasonably assumed to be much larger than that in the direction across the strait. Also, if the phenomena are confined near the Korean coast and if the Korean coast acts as a coastal waveguide on the rotating earth, the scale of the phenomena would be elongated in the direction of the wave propagation. So, we assume that the phenomenon can be

treated as a two-dimensional problem.

We use the Cartesian co-ordinate system as shown in Fig. 16, and take the x-axis horizontally in the cross-strait direction from the Korean coast, the y-axis horizontally along the Korean coast, and the z-axis vertically upward from the sea surface, respectively. The width of the strait is L, and the Japanese coast is located at x = L. The phenomenon is assumed to be two-dimensional, i.e. $\partial/\partial y = 0$. For simplicity, the water depth of the strait H is assumed to be constant.

Three types of the initial stratification will be examined in this study. Model 1 represents the summer stratification and Models 2 and 3 the winter stratification (see Fig. 16). The five layer system is adopted for Model 1 to describe the strong stratification in summer, and two layer system for Models 2 and 3 to describe the weak stratification. ρ_k is the density, and h_k the thickness of the k-th layer. Σh_i is H (i=1, 2, 3, 4, 5 for Model 1 and i=1, 2 for Models 2 and 3).

We denote the displacement of the upper boundary of the k-th layer with $\eta_k(x, t)$ and the transport (vertically integrated velocity) in the direction along the coast in the k-th layer with $V_k(x,t)$, respectively. By comparing the calculated distributions of η_k and V_k with the observed ones, we shall get the distribution of the sea surface elevation (η_1) under the presence of the bottom cold water. The water is assumed to be immiscible across the layer boundaries.

In the initial conditions, the fluid is at rest, and the bottom cold water is represented as a rectangular-shape upheave

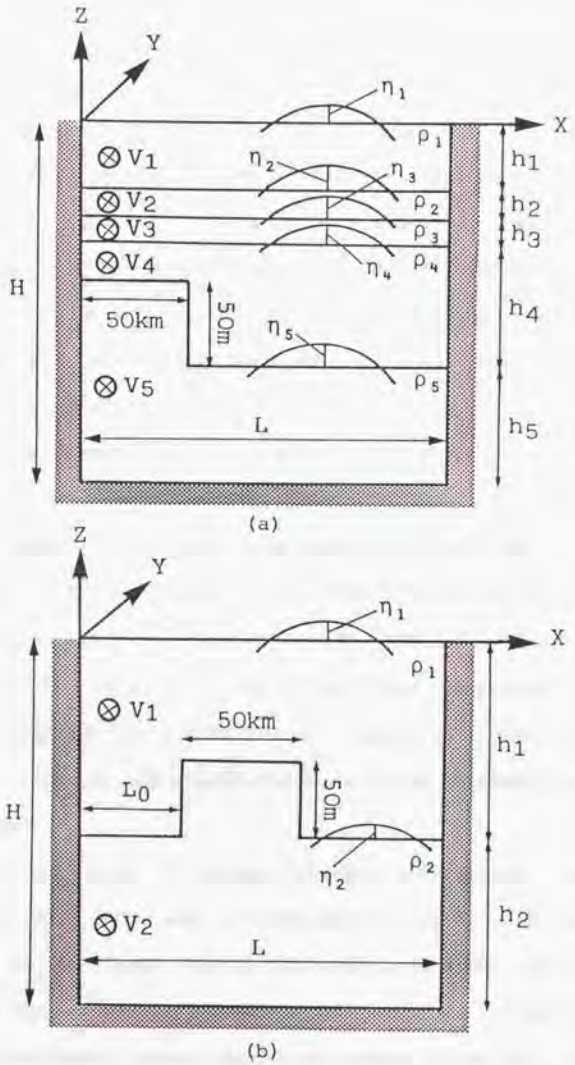

Fig. 16. Skematic view of the models and the initial shape of the upper boundary of the bottom cold water used in this study: (a) Model 1, and (b) Model 3. The stratification in Model 2 is the same as Model 3, but the initial position of the bottom cold water is the same as in Model 1. See the text for details.

of the upper boundary of the lowest layer. The bottom cold water is placed just off the Korean Coast in Models 1 and 2, while it is placed at the distance L0 apart from the Korean coast (see Fig. 16(b)). As seen in Figs. 5 and 7, the magnitude of the undulation of the upper boundary of the bottom cold water is 50- 100 m. In the models, the vertical scale of the upheave is taken as 50 m, and the horizontal scale as 50 km. Model 1 in Fig. 16(a) is assumed to represent the observed summer condition (Fig. 7: September 1990), and Model 3 in Fig. 16(b) the observed winter condition (Fig. 7: March 1991). Model 2 is used to check the influence of the position of the bottom cold water on the surface elevation. The stratification parameters used in the numerical experiments are shown in Table 2, together with several other parameters. These parameters in models are selected in a trial-and-error manner so as that the calculated velocity and density fields represent reasonably the observed ones.

The initial upheave of the upper boundary of the bottom cold water adopted is 50 m, and is large and comparative with the thickness of each layer, and the nonlinear terms would not be ignored in the equations of the motion. The non-linear advective terms are considered. Bottom friction is considered and given in quadratic form, but no friction is assumed along each interface. By assuming imcompressibility and by using hydrostatic approximation, we have the following horizontal momentum equations and the continuity equation:

Table 2 Parameters used in the numerical experiments

	Model 1	Model 2,3
Δt	10 sec	
ΔX	10 km	
H	250 m	
L	200 km	
f	0.83×10^{-4} sec^{-1}	
g	980 $cm \cdot sec^{-2}$	
γ	2.5×10^{-3}	
h_1	30 m	150 m
h_2	10 m	100 m
h_3	10 m	-
h_4	100 m	-
h_5	100 m	-
ρ_1	1.022 $g \cdot cm^{-3}$	1.025 $g \cdot cm^{-3}$
ρ_2	1.023 $g \cdot cm^{-3}$	1.026 $g \cdot cm^{-3}$
ρ_3	1.024 $g \cdot cm^{-3}$	-
ρ_4	1.0245 $g \cdot cm^{-3}$	-
ρ_5	1.027 $g \cdot cm^{-3}$	-
L_o	-	0 km(2), 50 km(3)

$$\frac{\partial U_k}{\partial t} + \frac{\partial}{\partial x}\left[\frac{U_k^2}{h_k+\eta_k-\eta_{k-1}}\right] + \frac{\delta\gamma(U_k^2+V_k^2)^{1/2}U_k}{(h_k+\eta_k)^2} - fV_k$$

$$= -\sum_{j=1}^{k}\left[\left(\frac{\rho_j-\rho_{j-1}}{\rho_k}\right)g(h_k+\eta_k-\eta_{k-1})\frac{\partial \eta_j}{\partial x}\right] \qquad (3\text{-}1)$$

$$\frac{\partial V_k}{\partial t} + \frac{\partial}{\partial x}\left[\frac{U_k V_k}{h_k+\eta_k-\eta_{k-1}}\right] + \frac{\delta\gamma(U_k^2+V_k^2)^{1/2}V_k}{(h_k+\eta_k)^2} + fU_k = 0 \qquad (3\text{-}2)$$

$$\frac{\partial(\eta_k-\eta_{k-1})}{\partial t} + \frac{\partial U_k}{\partial x} = 0 \qquad (3\text{-}3)$$

(k=1, 2, 3, 4, 5 for Model 1 and k=1, 2 for Models 2 and 3)

where U_k, and V_k are defined by

$$U_k = \int_{-h_k+\eta_{k-1}}^{\eta_k} u_k \, dz \quad ; \quad V_k = \int_{-h_k+\eta_{k-1}}^{\eta_k} v_k \, dz \qquad (3\text{-}4)$$

and $u(x,z,t)$ and $v(x,z,t)$ are the x- and y-components of the velocity. g is the gravitational acceleration, f the Coriolis parameter and γ the bottom drag coefficient. $\rho_0 = 0$, $\eta_0 = 0$ for Model 1, and $\eta_2 = 0$ for Models 2 and 3. $\delta = 0$ except for the bottom layer ($k = 5$ for Model 1 and $k = 2$ for Models 2 and 3) where δ is taken to be 1. The boundary condition imposed is that the velocity components normal to the coast in each layer vanish at the coast walls ($x = 0$ and $x = L$). Equations (3-1)-(3-3) are converted into a finite difference scheme by applying the centered difference and leap-frog scheme with a time increment Δt. To suppress numerical instability, the

Euler-backward scheme is applied every 20 time steps. The evolution of the velocity and density structures in the strait is numerically calculated under the initial and boundary conditions described above.

The calculated structures achieve almost a quasi-steady state after one inertia period (around 21 hours at 35°N). In our experiments, time integration was carried out for ten inertia periods (around 8 days). The calculated results usually exhibit short period fluctuations, and the averaged fields for the last 21 hours are used for the following discussions.

3.3 RESULTS OF EXPERIMENTS

3.3.1 The distribution of the surface elevation in the summer season

For the case of Model 1 (the summer state), the calculated cross-strait distributions of the displacements of the upper boundary and of the averaged current component $u_k(x)$ parallel to the coast are given for each layer in Fig. 17(a). The averaged current component is defined by $v_k = V_k/(h_k + \eta_k - \eta_{k-1})$.

It can be seen that the displacement of the upper boundary of the bottom cold water (η_n) decreases monotonically from the Korean coast to the Japanese coast, and the most sharp gradient occurs at x = 50 km where we set the offshore boundary of the bottom cold water in the initial condition. The resulted configuration roughly corresponds to that of the main thermocline shown in Fig. 5.

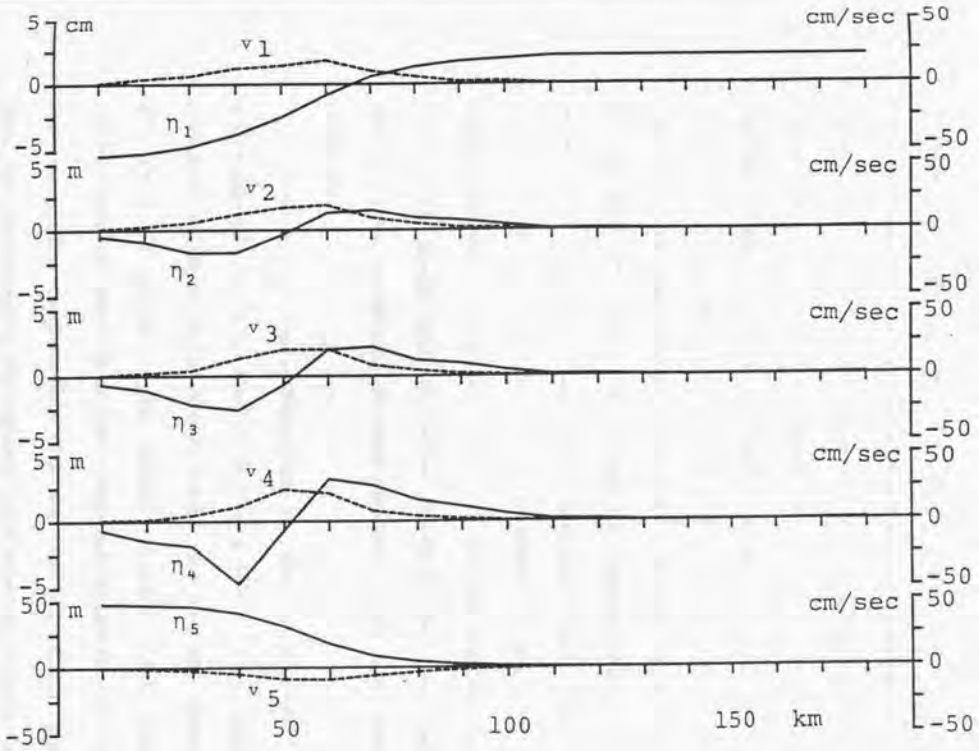

(a)

Fig.17. The shapes of the surface/interface elevation (full line: see the left ordinate for its scale) and of the northeastward component of the velocity parpendiculer to the section (broken line: see the right ordinate for its scale) after a qusi-steady state is achieved: (a) for the Model 1, (b) Model 2 and (c) Model 3. Note that the vertical scale for the displacement is changed figure by figure.

η_2 and η_4 correspond to the upper and lower boundaries of the seasonal (first) thermocline, respectively, and η_3 are set to represent the sharpness of the summer thermocline. These interfaces are lowered near x = 40 km and heaved near x = 70 km. Such S-shaped configuration is seen for the observed seasonal thermocline, halocline and pycnocline shown in Fig. 5,6 and 7, respectively. It should noted that the positions of depression and upheave in the model correspond well with those observed ones. The amplitude of the undulation of the calculated seasonal thermocline reaches about 5 m (±5 m: see the profile of η_4 in Fig. 17), while the observed amplitude is about 10 m between at Sta. 5 and Sta. 7 in 11 September, 1990 (see Fig. 5). In our model, the upheave of the upper boundary of the bottom cold water is assumed to be 50 m, but the observed upheave is a little larger than this value (50-100 m). So, our modeled results seem to show fairly good agreement with the observed situation.

According to the deformation of the thermocline, the northeastward currents (v_2-v_4) in the middle layers appeared around at x = 50 km in the middle layers, and have the magnitude of about 20 cm·sec^{-1}. The counter current (v_5) flowing southwestward of about 10 cm·sec^{-1} appeared in the bottom layer. The intensified current zone with high vertical shear appears well to correspond to the current field near the Korean coast observed by ADCP survey in September 1990 (see Fig. 13(a)).

The northeastward current of about 15 cm·sec^{-1} is seen also in the surface layer around at x = 50 km, though the width of the

current zone is widen in comparison with in the middle layer. The resultant configuration of the sea surface (η_1) is monotonically increases from the Korean coast to the Japanese coast. The sea level is lowered by about 5 cm at the Korean coast (x=0 km). The sea level difference across the Strait is about 8 cm. It should be noted that the sea level is very flat in the Eastern Channel, and that sea level gradient can be seen in the Western Channel between x=0 and x=100 km.

3.3.2. The distribution of the surface elevation in the winter season

In Model 2, the stratification is changed into the winter state, but the position and the shape of the initial bottom cold water are just the same as in Model 1. The calculated cross-strait distributions of the displacements of the upper boundary and of the averaged current component parallel to the coast are given for each layer in Fig. 17(b).

As the vertical density gradient is weakened in the winter stratification, and as the internal radius of deformation is smaller, the displacement of the upper boundary of the bottom cold water (η_2) is more confined near the initial offshore boundary of the bottom cold water (x = 50 km) in comparison with the result in Model 1.

The northeastward current (v_1) of about 10 cm·sec^{-1} appeared in the upper layer, and the southwestward current(v_2) of about 5 cm·sec^{-1} appeared in the bottom layer. The width of the current zone in each layer is narrower than that of the Model 1.

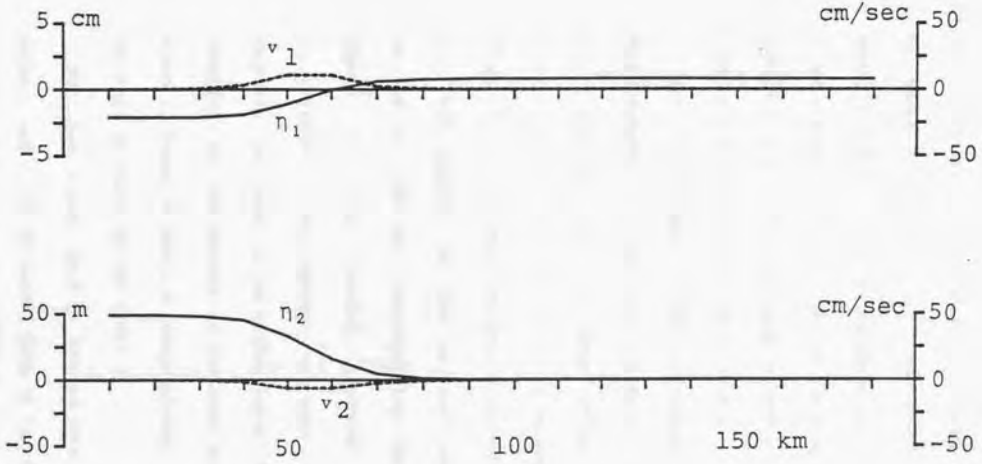

(b)

Fig.17 (continued)

The sea level (η_1) is lowered by about 2 cm at the Korean coast, and the sea level difference across the Strait is about 3 cm in Model 2. The depression of the sea level occurs on the left-hand side of the Strait (the Western Channel) as in Model 1. In Model 3, the position of the initial bottom cold water is moved offshore by 50 km as shown in Fig. 16(b). The calculated cross-strait distributions of the displacements of the upper boundary and of the averaged current component parallel to the coast are given for each layer in Fig. 17(c).

The both edges of the rectangular shape of the initial displacement of the upper boundary of the bottom cold water are smoothed and the shape of η_2 becomes a bell-shape after adjustment process just as seen in the observed one (Fig. 5). The weak northeastward and southwestward currents (v_1, v_2) appear in the surface layer around at x = 50 km and at 100 km corresponding the inshore and off shore edges of the initial upheave of the interface, respectively. The counter currents corresponding to these currents are seen in the bottom layer. The magnitudes of the velocity of the current in the both layers are of the same order of those in Model 2, respectively. These values are about the half of those in the Model 1.

The sea level (η_1) is lowered just above the bottom cold water, and it is raised both at the Korean coast and at the Japanese coast. The maximum displacement of the sea level occurs at x = 80 km and its magnitude is 2 cm. This value is also about the half of the maximum displacement in Model 1.

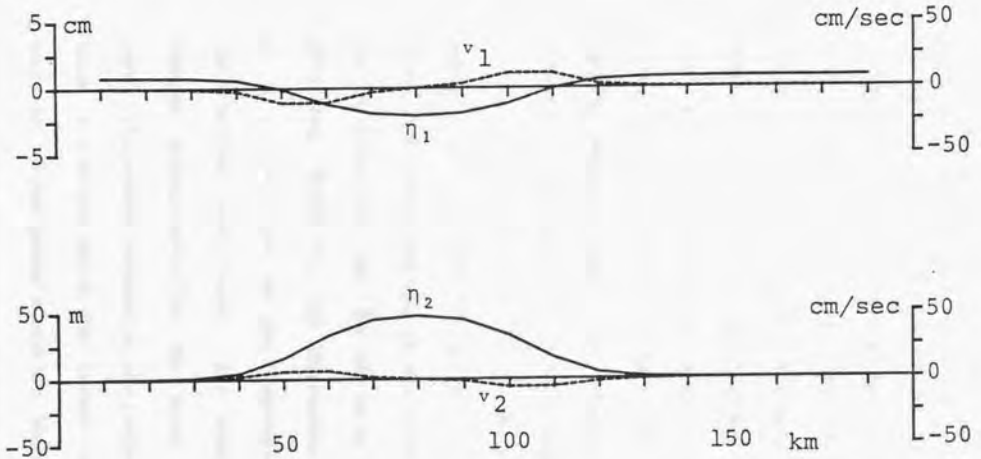

(c)

Fig.17 (continued)

3.3 DISCUSSIONS

- The magnitude of the seasonal sea level variation -

The results of the model calculation indicate that the existence of the bottom cold water yields considerable influence on the sea level distribution across the Tsushima Strait, and that the resultant sea level difference across the strait is of order of 8 cm in summer (Model 1). The sea level gradient is very significant near the Korean coast or in the Western Channel. When the stratification is weakened in winter, the sea level difference across the strait decreases to of order of 3 cm (Model 2), if the position of the bottom cold water is just off the Korean coast just as in the summer case. If the position of the bottom cold water is shifted southeastward by 50 km so as to fit the observed winter situation (Model 3), the depression portion of the sea level moves southeastward as the depression occurs just above the bottom cold water. Its magnitude, however, is not changed significantly for the given parameters, and the sea level difference between at the center of the bottom cold water (x = 80 km) and at the Korean coast is about 3 cm. In contrast to the summer condition, the sea level at the Korean coast is predicted to rise in winter by about 1 cm. It should be noted that the sea level at the Japanese coast rises about 2 cm in summer and 1 cm in winter. The winter situation modeled in Model 3 does not arise significant sea level

difference across the whole Tsushima Strait. As many investigators (e.g., Hidaka and Suzuki 1950, Kawabe 1982) indicated, the seasonal variation in the transport or the current velocity in the Tsushima Strait occurs in the Western Channel, we shall confine our discussions mainly to the Western Channel (say, between x =0 and x = 80 km).

Kawabe (1982) pointed out that the range of the seasonal variation of the sea level difference across the Western Channel reaches about 15 cm. The sea level difference across the Western Channel is 8 cm in summer (Model 1) and -3 cm in winter (Model 3), and the range of the seasonal variation is 11 cm. (Note that the 50 m upheave of the upper boundary of the bottom cold water might be underestimation as discussed before.) The predicted range 11 cm is almost comparable with the observed one, 15 cm. (The range averaged for the period from 1988 to 1990 is 12 cm as will be discussed in the next section). This means that the existence of the bottom cold water or the baroclinic nature in the Western Channel gives considerable influence on the sea level difference and that the sea level difference across the channel may not give a good information for the seasonal variation of the transport or current velocity in the Tsushima Strait.

It should be noted that the position of the bottom cold water is essential to create such a large sea level difference. If the bottom cold water is located just off the Korean coast in winter as just as in summer, the range of the seasonal variation is only about 5 cm (compare the results of Model 1 and Model 2). As

discussed in the previous sub-section, the internal radius of deformation is smaller in winter. The influence of the initial upheave of the upper boundary of the bottom cold water is confined to rather narrow domain, and does not reach to the Korean coast within the experimental parameter range. We did not check the dependence of the sea level difference on the position L_0, but the configurations of the sea levels in Fig. 17 would give some ideas on this effect. The sea level measurements are most feasible for long-term monitoring of the oceanic condition, and the sea level difference across the strait contains the information for the transport or the surface velocity through the strait. In the next section, we shall try to estimate the seasonal variations of the transport of the Tsushima Warm Current in the Tsushima Strait by combining the data of sea level difference and of hydrographic observations. We hope that the result may help to find the possible way to remove the baroclinic influence from the observed sea level difference in order to use the sea level difference informations for the long-term monitorring of the Tsushima Warm Current in the Tsushima Strait in future.

4. *ESTIMATION OF THE NET TRANSPORT OF THE TSUSHIMA WARM CURRENT AND ITS SEASONAL VARIATION*

4.1 DATA AND ANALYSIS PROCEDURE

4.1.1 Sea level data

The sea level data at Hakata, Izuhara and Pusan have been used by many investigators to estimate the seasonal variation of the transport of the Tsushima Warm Current in the Tsushima Strait (See Fig. 3 for the location of these tidal stations). The daily mean sea level data at these stations from 1988 to 1990 were used by courtesy of the Japan Oceanographic Data Center.

In Fig. 18, the sea level difference between Izuhara and Pusan (the Western Channel: the upper figure), and between Hakata and Izuhara (he Eastern Channel: the lower figure) are given for the analyzed period from 1988 to 1990. The relative height of the datum levels between in Korea and in Japan is not known, and the sea level difference is measured from the three year averaged sea level difference for each channel. The barometric adjustment was not conducted because the distances between stations are only about 100 km and atmospheric pressure differences between the stations would be small in typical conditions. The sea level difference across the Western Channel shows a remarkable seasonal variation with the range of about 12 cm, whilst distinct seasonal variation is not seen in the Eastern Channel. The variation range in the Western Channel is a little smaller than that given by Kawabe (1982) as a averaged value for

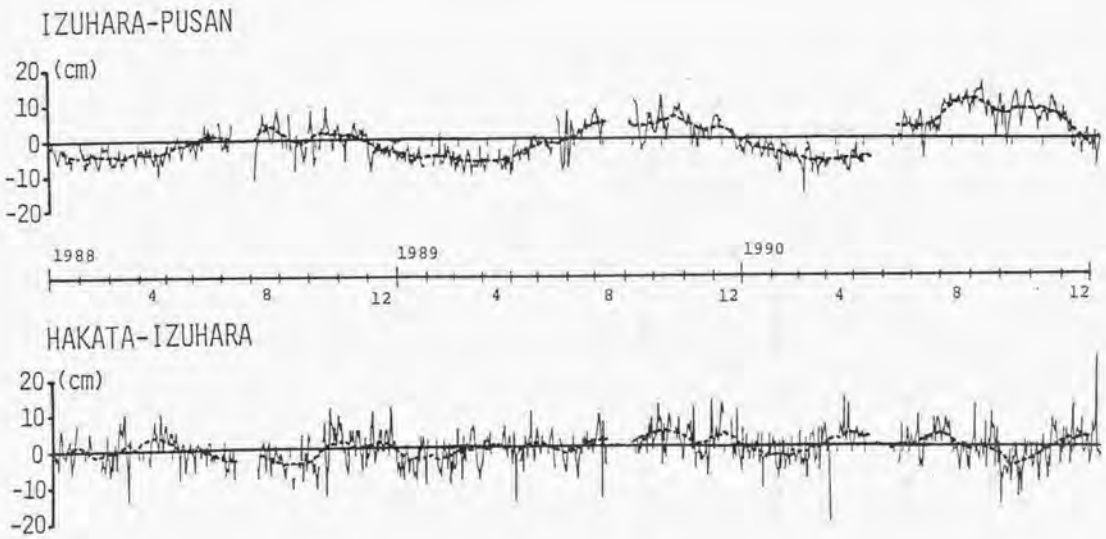

Fig.18. The temporal variations of the differences in daily mean sea level between Izuhara and Pusan (the upper figure) and between Hakata and Izuhara (the lower figure) from 1988 to 1990. The broken line shows the 30-day running mean. The differences are obtained by subtracting the value at Pusan from that at Izuhara for the upper figure, and the value at Izuhara from that at Hakata for the lower figure. The zero line corresponds the averaged sea level difference in the analyzed period.

Table 3 Date of the CTD casts or the dynamical computation

1988	5 Apr., 10 May, 7 June, 3 Aug., 2 Sept. 1 Nov., 2 Dec.
1989	14 Mar., 10 May, 4 Jul., 7 Sept., 5 Oct. 15 Nov.
1990	6 Mar., 11 Apr., 4 Jul., 3 Aug., 5 Sept. 11 Sept., 3 Oct., 31 Oct.

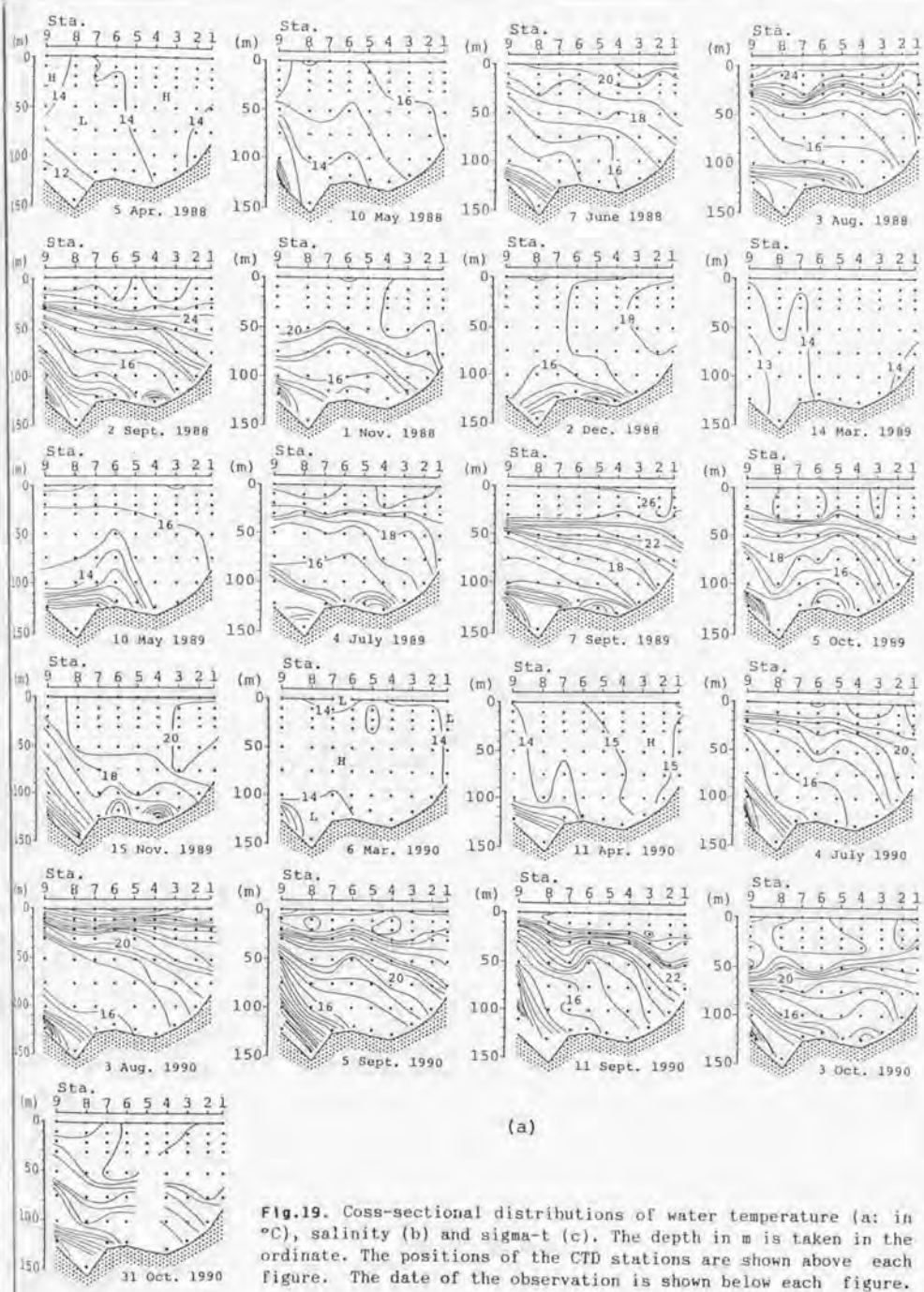

(a)

Fig.19. Coss-sectional distributions of water temperature (a: in °C), salinity (b) and sigma-t (c). The depth in m is taken in the ordinate. The positions of the CTD stations are shown above each figure. The date of the observation is shown below each figure.

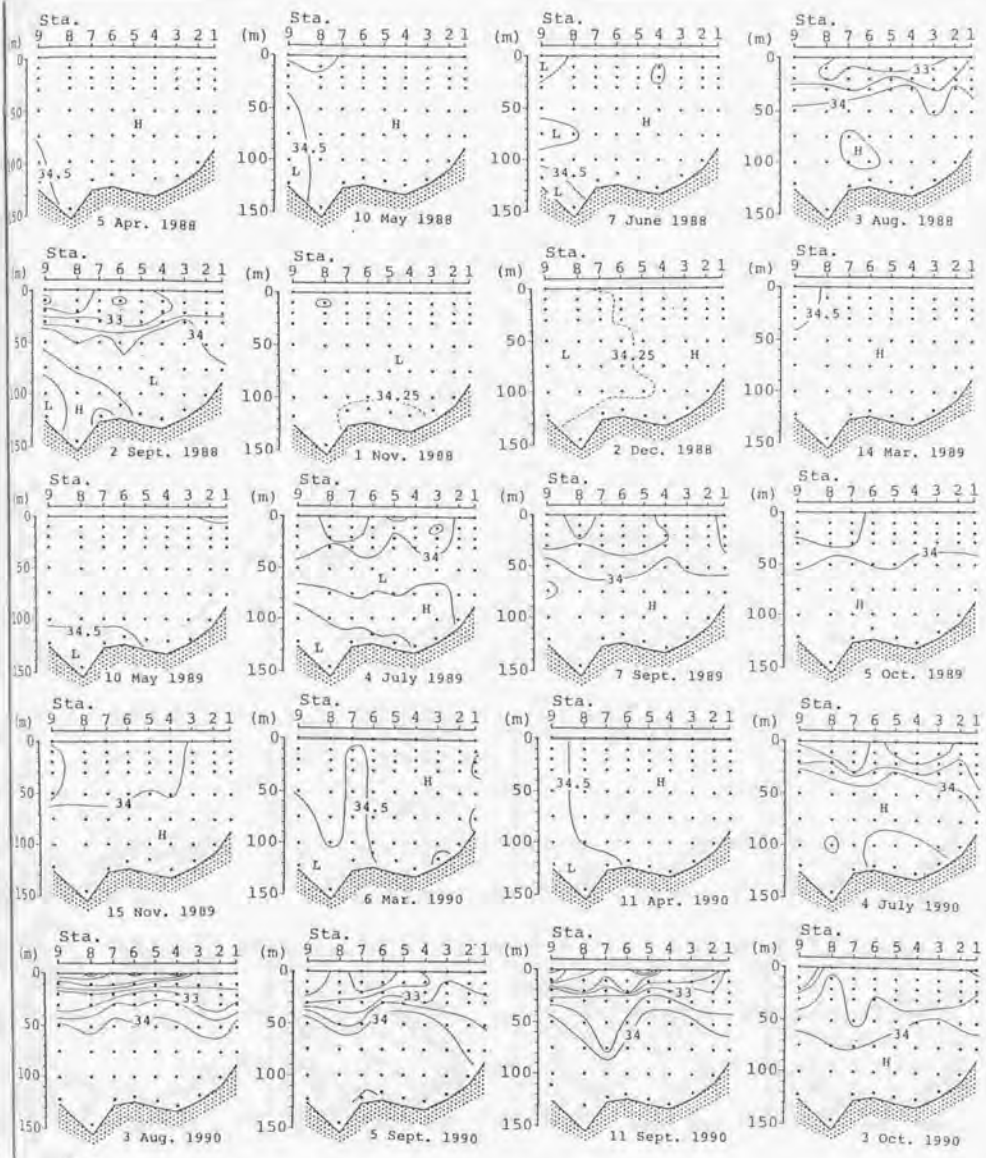

(b)

Fig.19 (continued)

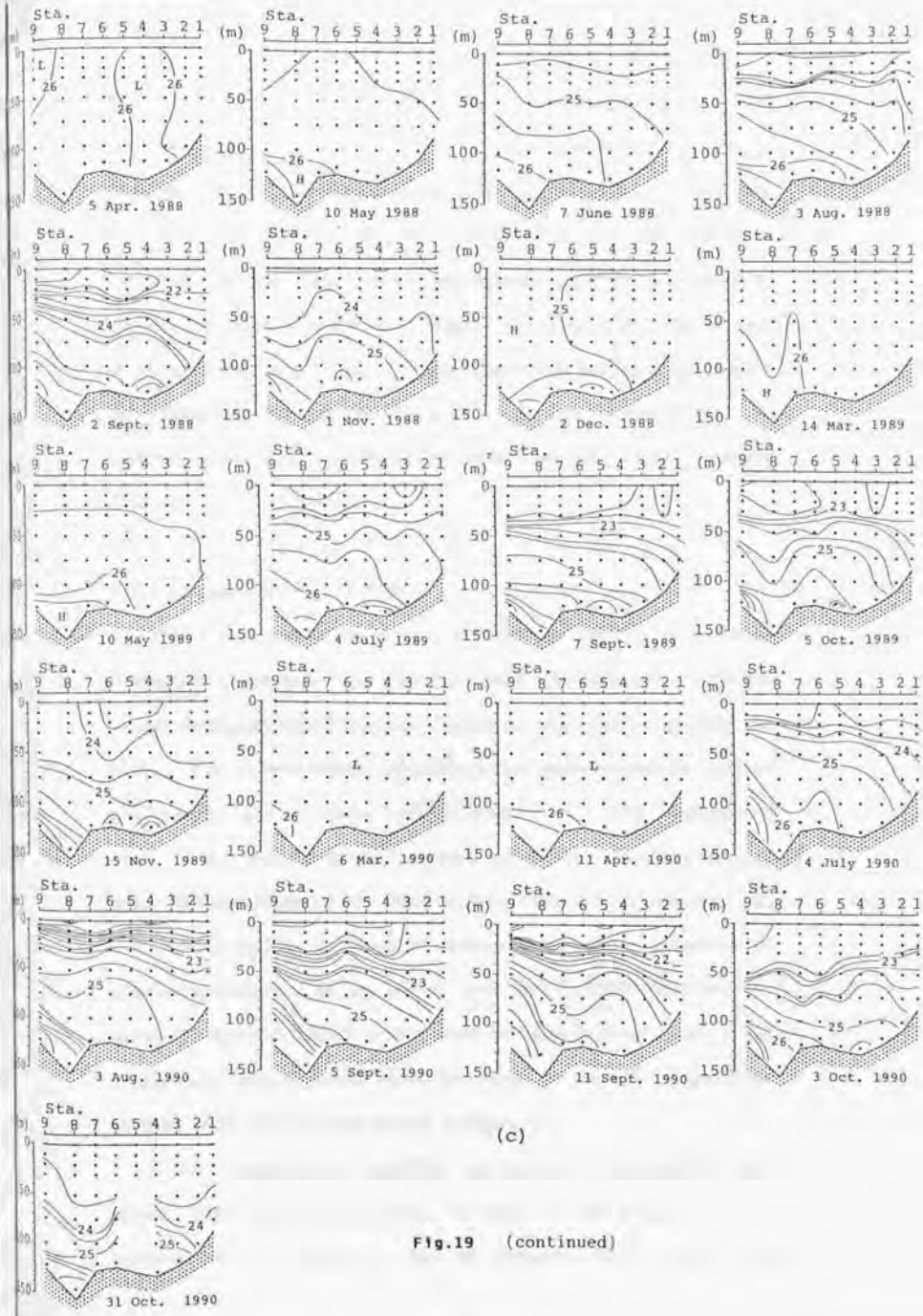

(c)

Fig.19 (continued)

the period from 1966 to 1976. However, the gross features of the variation characteristic in both channels are very similar to those discussed by various investigators (Hidaka and Suzuki 1950, Yi 1966, and Kawabe 1982). The temporal variation of the sea level differences in Fig. 18, however, should be influenced by the variation in baroclinic structures as discussed in the previous section, and cannot be related directly to the variation of the transport and the current velocity of the Tsushima Warm Current in the Tsushima Strait.

4.1.2 Hydrographic (CTD) data

The CTD observations across the Tsushima Strait have been conducted routinely by the Yamaguchi Prefectural Open-Sea Fisheries Experimental Station. Though no observation is made in Korean territorial water, and though the observations in winter are seldom due to severe weather conditions, this observation line is the most frequently covered one in the Tsushima Strait area. The positions of the observations, Stas. 1 through Sta. 9, are shown in Fig. 3. About 30 cruises along this observation line were conducted in the period from 1988 to 1990. However, we used CTD data of the 21 cruise when the simultaneous sea level difference data are available. The dates of the CTD observation used in this analysis are shown in Table 3.

The temperature, salinity and sigma-t distributions are shown for all observations in Table 3 in Figs. 19 (a: temperature), (b:salinity) and (c: sigma-t). The bottom cold

water is always found near the Korean coast throughout the analyzed period, though its cross-sectional area and the sharpness of the main thermocline are very changeable seasonally and interannually. The offshore shift of the position of the bottom cold water in winter-spring discussed in the Section 3 is clearly seen in the sections on 2 December 1988 and on 10 May 1989. But the situation is very changeable year by year and the shift is not so clear in other winter sections. It may be anticipated from the cross-sections shown in Fig. 19 that the baroclinic motion is predominant especially in the Western Channel, and that its nature is very changeable. So, the sea level difference induced from the baroclinic current would be large and be changeable seasonally and interannually in the Western Channel.

The seasonal thermocline is well developed in summer-autumn, and there is a general tendency to decline towards the Japanese coast. Its sharpness and the configuration is changeable again both seasonally and inter-annually, especially in the Eastern Channel. The influence of the baroclinic currents on the sea level distribution would be significant, at least, in the Eastern Channel.

4.1.3 The procedure to obtain sea surface distribution due to baroclinic current component

To obtain the sea level difference associated only with the barotropic mode of the oceanic structure, we need to subtract the sea level difference associated with the baroclinic

mode from the observed sea level difference. In this paper, the sea level difference associated with the baroclinic mode is calculated as follows.

Take A and B as two neighboring stations where the vertical distribution of the density was observed (Fig. 20). We take the x-axis southeastward along the observation line, the y-axis northwestward, and z-axis vertically upward from the sea surface. The current is assumed to flow in the y-direction. We shall define the baroclinic current component so as that its vertically integrated value from the sea surface to the bottom vanishes. To obtain the baroclinic current from the observed vertical density profiles, we first seek the reference depth (z=-R) where the baroclinic component becomes zero (Fig. 20) by using the following relation:

$$\frac{1}{f\Delta X}\int_{-H}^{0}\left[(\Delta D_B-\Delta D_A)_{-R}-(\Delta D_B-\Delta D_A)_Z\right]dz = 0 \qquad (4\text{-}1)$$

where f is the Coriolis parameter (=8.34x10^{-5}sec^{-1},35°N), H the mean depth, ΔX the distance between Stas. A and B, $\Delta D_A(z)$ and $\Delta D_B(z)$ the dynamic depth anomaly calculated from CTD data at Sta. A and Sta., B, respectively. The subscripts -R and Z indicate that the values should be estimated at the depths -R and Z, respectively. In the area under consideration, the oceanic structure is simple enough that the current profiles satisfying the equation (4-1) has a form as schematically shown with dotted curve in Fig. 20. Then, the surface current velocity (V_o) of the

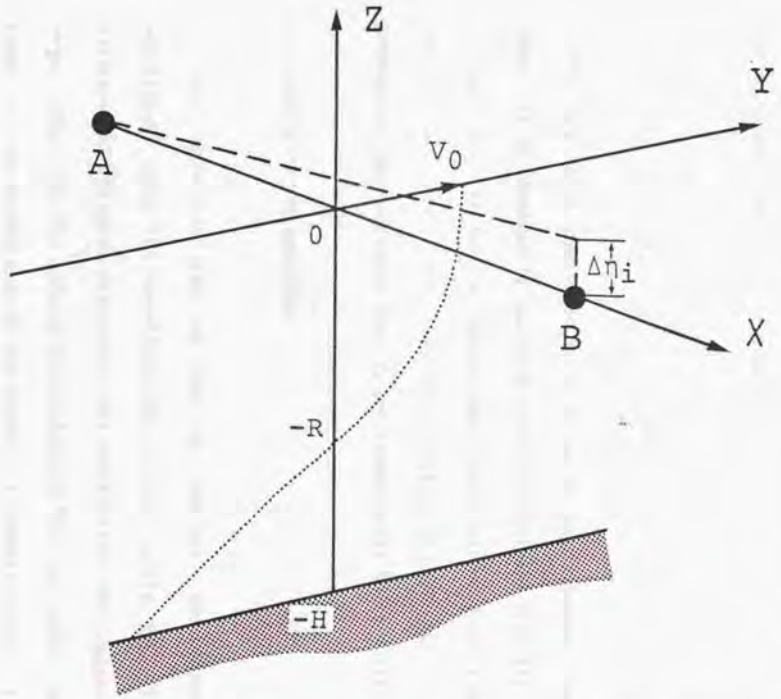

Fig.20. Model used to calculate the baroclinic current profile (dotted line), the baroclinic surface speed (V_o) and the sea level gradient $\Delta\eta_i$ between the neiboring satations A and B. See the text for details.

baroclinic mode is given by

$$V_0 = \frac{1}{f\Delta X}(\Delta D_B - \Delta D_A)_{-B} \qquad (4\text{-}2)$$

The sea level difference associated with the baroclinic mode ($\Delta\eta_1$) between A and B is obtained by

$$\Delta\eta_1 = \frac{f}{g}\,\Delta X\, V_0 \qquad (4\text{-}3)$$

The sea level distribution relative to the Japanese coast (Sta. 1) is obtained by applying (4-3) successively from Sta. 1 to Sta. 9. We have no hydrographic data between Sta. 9 and the Korean coast, and the sea level at Sta. 9 will be considered to represent that at the Korean coast in this paper.

4.2 RESULTS OF THE ANALYSIS

The space-time plot of the sea surface displacement associated with the baroclinic mode is shown in Fig. 21. The displacement is given relative to the sea level at the Japanese coast (Sta. 1). The intense depressions of the sea level are found on the Korean side of the Strait in summer-autumn. Its magnitude exceeds 5 cm every year, but is very large in 1990 (July and September) and exceeds 10 cm.

The bottom cold water exists usually to the west of Sta. 6, and the eddy-like structure, which might be generated on the lee

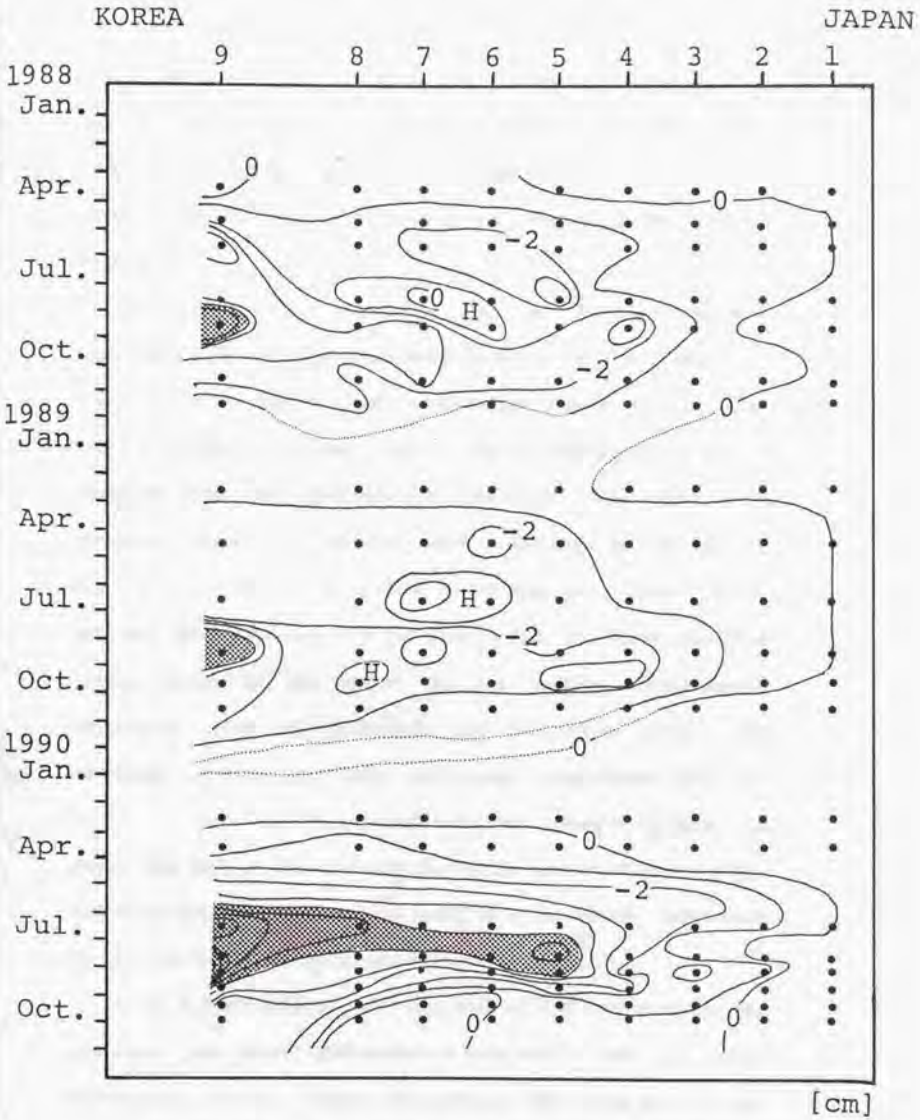

Fig.21. The temporal and spatial variation of the baroclinic sea level. The sea level is plotted relative to that at the Japanese coast. The contour interval is 1 cm. The shaded area indicates the domain where the sea level lower than -5 cm.

side of the Tsushima Island, is often observed near at Sta. 6. We shall divide the strait into two regions to the west of and the east of this station conventionally. The former region (from Sta. 6 to Sta. 9) will be considered as the Western Channel and the latter (from Sta. 1 to Sta. 6) as the Eastern Channel.

The temporal variations of the sea level difference associated with the baroclinic mode (black circles) are shown in Fig. 22 for the Western Channel (the upper figure) and for the Eastern Channel (the lower figure). The sea level difference is measured from the mean values for analyzed three years. The observed sea level differences taken on the same day of the CTD observations are picked up from 30-day mean sea level data, and are shown with open circles also in Fig. 22. These observed values should be the sum of the sea surface displacements associated with the barotropic and baroclinic modes. The variation of the sea level difference associated with the baroclinic mode has similar magnitude and changes roughly in phase with that of the observed one in the Western Channel. This indicates that the observed sea level is considerably influenced by the baroclinic motion in the Western Strait.

In the Eastern Channel, the amplitude of the variation of the observed sea level difference is very small, and sea level difference varies rather irregularly. The variation of the baroclinic sea level difference (black circles in the lower figure in Fig. 22), however, tends to slightly increase in summer and to decrease in winter. This would be resulted from

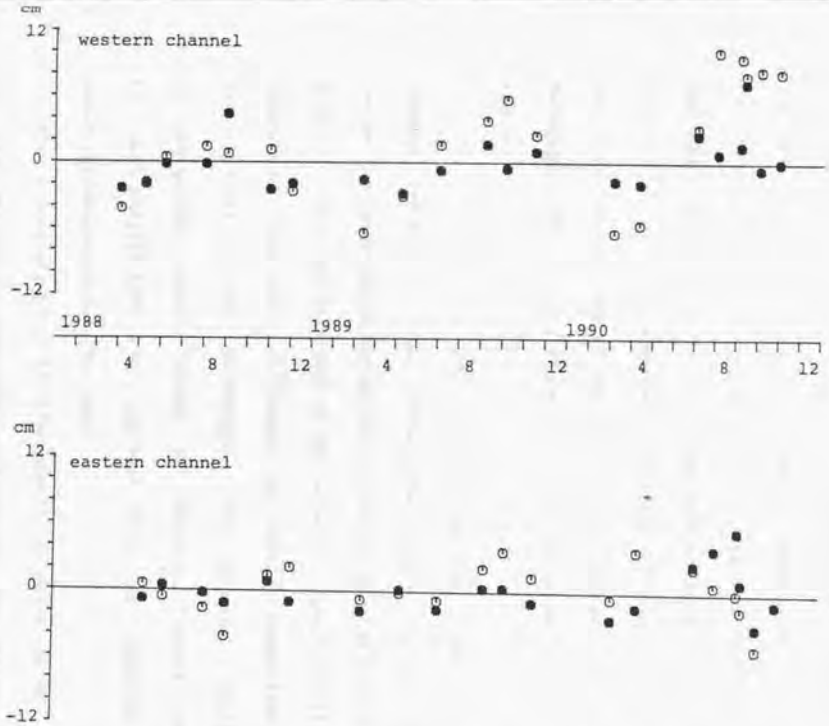

Fig.22. Temporal variations of the sea level difference (in cm) across the Western Channel (the upper figure) and across the Eastern Channel (the lower figure). The baroclinic sea level difference is shown with a black circle, and the observed sea level difference (30-day running mean) with a open circle. The data for the observed sea level difference are shown only when the baroclinic sea level difference data are available.

the variation of the thermocline structure near the Japanese coast.

The temporal variation in the due sea level difference (the barotropic sea level difference) which is associated only with the barotropic component of the current is obtained by subtracting the sea level difference associated with the baroclinic mode from the observed sea level difference. The barotropic sea level difference calculated are shown in Fig. 23. The variation of the barotropic sea level difference, $\Delta\eta$ can be converted into that of the total volume transport, Q by the relation, $Q = (g/f)(\Delta\eta)H$ (H is the mean depth of the channel).

The barotropic sea level difference or the volume transport through the Western Channel takes higher values during summer-autumn and lower values during winter-spring. It should be noted, however, that the magnitude of the seasonal variation of the barotropic sea level difference decrease in comparison with the observed sea level difference. The seasonal variation of the volume transport through the Western Channel should be much smaller than that expected from the observed sea level difference across the channel.

The strong signal of the interannual variation can be seen in Fig. 21, and the cross-sectional area of the bottom cold water was abnormally large in 1990. The barotropic sea level difference was very large in the summer-winter of 1990. This might be related to the abnormal oceanic condition occurred in 1990.

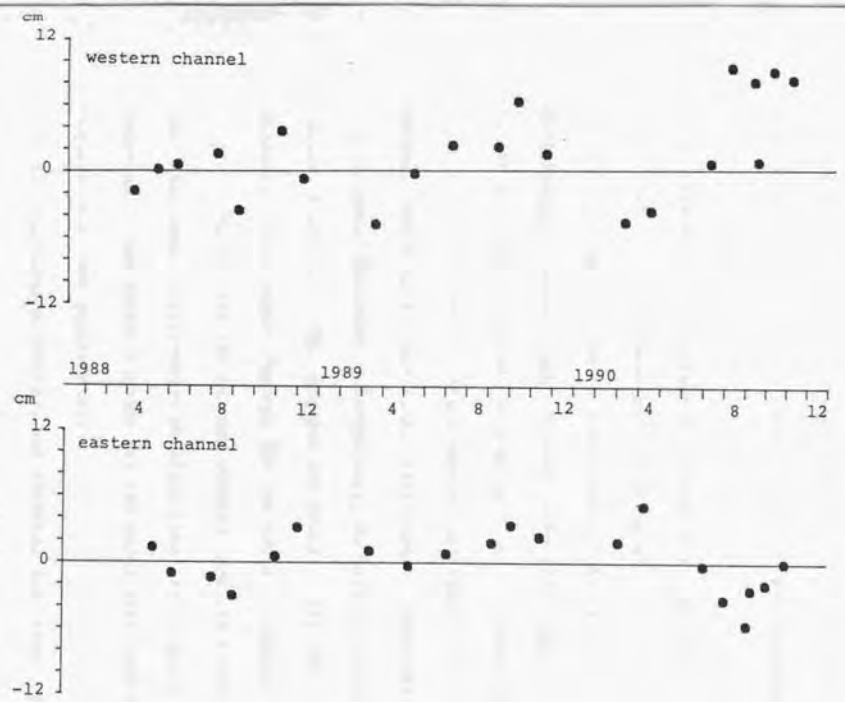

Fig.23. The same as in Fig. 22, except fot the barotropic sea level differences.

In the Eastern Channel, the barotropic sea level difference tends to increase in winter and to decrease during summer.

4.3 DISCUSSIONS

-The nature of the seasonal variation of the Tsushima Warm Current in the Tsushima Strait-

To eliminate the interannual variations and to obtain the gross nature of the seasonal variation of the Tsushima Warm Current transport, the obtained three kinds of the sea level differences across each channel (observed, baroclinic and barotropic) are aligned in order of the observed month by ignoring the observed year, then are averaged for every two months; March-April, May-June, July-August, September-October, and November-December. Unfortunately, no data is available for January-February. The results are shown in Fig. 24 for both channels (the upper figures for the Western Channel and the lower figures for the Eastern Channel) and for three kinds of the sea level differences obtained (the left figures for the observed, the center figures for the baroclinic, and the right figures for the barotropic).

In the Western Channel, the observed sea level difference has a seasonal variation of the magnitude of about 12 cm (the upper left figure in Fig. 24). If the effects of the baroclinic sea level difference is ignored, this would indicate that the range of the seasonal variation in volume transport through the Western Channel is of order of 2 Sv. However, the contribution to

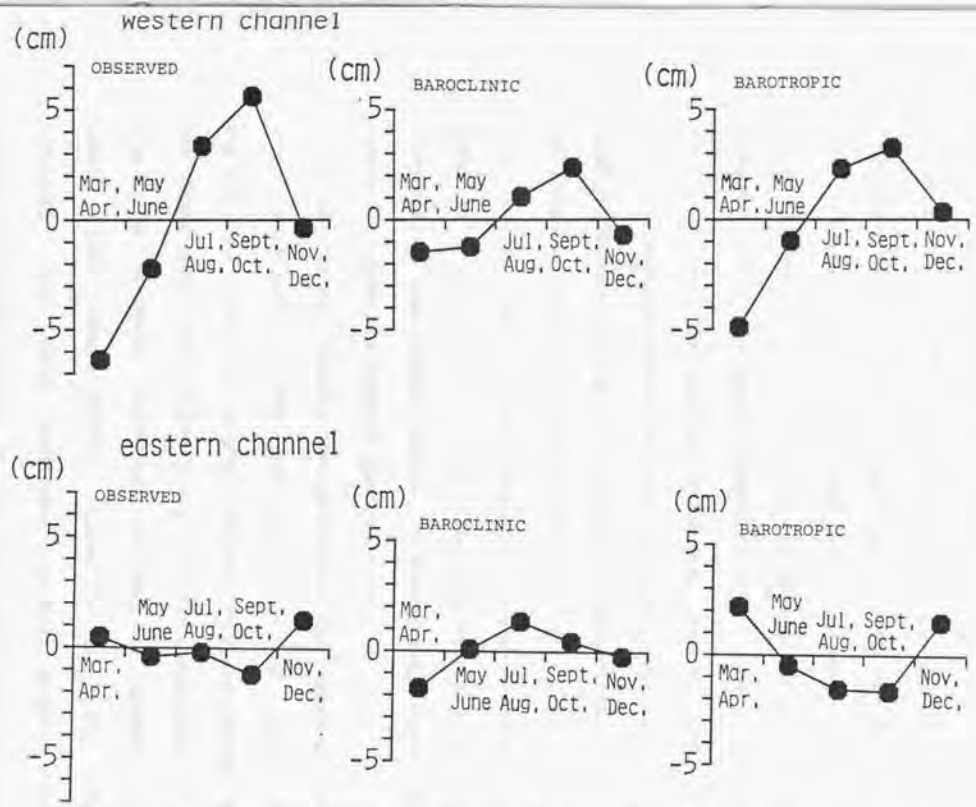

Fig.24. Seasonal variations of the observed sea level differences (the left culumn), the baroclinic sea level difference (the central column) and the barotropic sea level difference (the right column) across the Western Channel (the upper figure) and across the Eastern Channel (the lower figure).

the sea level difference from the baroclinic motions is significant as seen in the upper central figure in Fig. 24. We need to make a correction to remove it. The real seasonal variation should be estimated from the barotropic sea level difference shown in the upper right figure of Fig. 24. The range of the seasonal variation of the barotropic sea level difference is about 8 cm, and the resulted variation range in the volume transport through the Western Channel is about 1.3 Sv (0.65 Sv in amplitude). For the analyzed period from 1988 to 1990, the seasonal variation of the barotropic sea level difference (the upper right figure in Fig. 24) is roughly in phase with that of the observed sea level difference (the upper left figure in Fig. 24). If this relation holds in general, the observed sea level could be a good index for monitoring the variation of the transport in the Western Channel. Further investigations are needed to check the relation quantitatively.

In the Eastern Channel, the variation of the observed sea level difference is very small (the lower left figure in Fig.24), but tends to slightly decrease in summer-autumn. On the other hand, the baroclinic sea level difference shows a significant seasonal variation, and tends to increase in summer (the lower central figure in Fig. 24). The barotropic sea level difference exhibits rather clear seasonal variations as seen in the lower right figure in Fig. 24, indicating that the transport through the Eastern Channel increases in winter.

Tawara and Fujiwara (1985) analyzed the sea surface

temperature across the Tsushima Strait, and reported that a cold water always exists near the coast of Kyushu in winter. Such cold water can not be identified in the temperature cross-sections shown in Fig. 19(a), and may be a narrow coastal phenomena. However, when the water is a considerably thick, the cold water has the effect to lower the sea level in winter. Since this effect is not included, the amplitude of the seasonal variation of the baroclinic sea level difference across the Eastern Channel might be a little bit underestimated in our analysis.

The total volume transport flowing into the Japan Sea is the sum of the volume transports of the Western and Eastern Channel. The seasonal variation of the barotropic sea level difference across the whole Tsushima Strait is shown in Fig. 25. The range of the seasonal variation of the total volume transport through the whole Tsushima Strait is 0.7 Sv. This value is smaller than that through the Western Channel, as the variation in the Eastern Channel is out of phase to that in the Western Channel.

The seasonal variations of the observed sea level difference across the strait and the bottom referred geostrophic transport obtained from the observed density distribution are shown also in Fig. 25 for comparison. It should be noted that the amplitude of the barotropic sea level difference is much smaller than and is from 1/3 to 1/2 of that of the observed sea level difference (or that of the corresponding geostrophic transport).

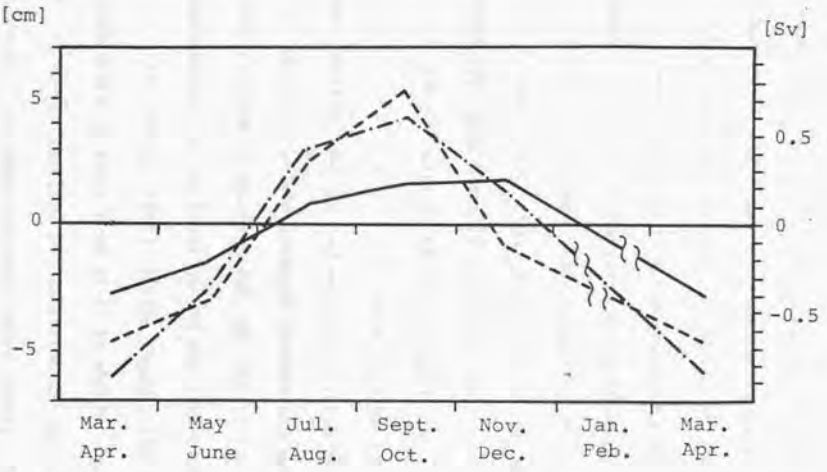

Fig. 25. Seasonal variation of the barotropic sea level difference (in cm, see the left ordinate: the solid line) across the whole Tsushima Strait. The corresponding value of the transport in Sv is taken along the right ordinate. The observed sea level difference (in cm, see the left coordinate: dash-dotted line) across the strait and the bottom-referred geostrophic transport (in Sv, see the right coordinate: dashed line) obtained from the density distribution shown in Fig. 19, are also shown in the figure.

The total volume transport takes a maximum in early winter (November-December), and a minimum in spring (March-April). The similar tendency is shown for the surface current velocity by Egawa eta al. (1993), who analyzed the data of direct current measurement (ADCP data). It should be also noted that the phase of the seasonal variation of the total transport is different from that estimated from the observed sea level difference as shown in Fig. 25. This gives an explanation why other previous investigators (Hidaka and Suzuki, 1950; Yi, 1966; Kawabe, 1982; Toba et al., 1982) argued that the maximum total volume transport takes place in summer-autumn.

In the discussions above, we emphasized the importance of the bottom cold water and its variability on the current system in the Western Channel and on the sea level at the Korean coast. The variation of the vertical temperature profile at Sta.9 from 1988 to 1990 is shown in Fig. 26. The bottom cold water may be represented by the water having the temperature lower than 10 °C (Lim and Chang, 1969). In the figure, the portion where the temperature is lower than 10 °C is shaded, and that lower than 5 °C is shaded heavily. The intrusion of the bottom cold water is enhanced in summer-autumn every year. This summer-autumn intrusion is most remarkable in 1990, and the cross-sectional area and the horizontal extent of the bottom cold water are also large in summer-autumn in 1990 (see Fig. 19(a)). The intrusion phenomenon and its variability can be traceable also in the space-time diagram of the sea level displacement in Fig. 21. The depression at the Korean coast exceeds 10 cm in

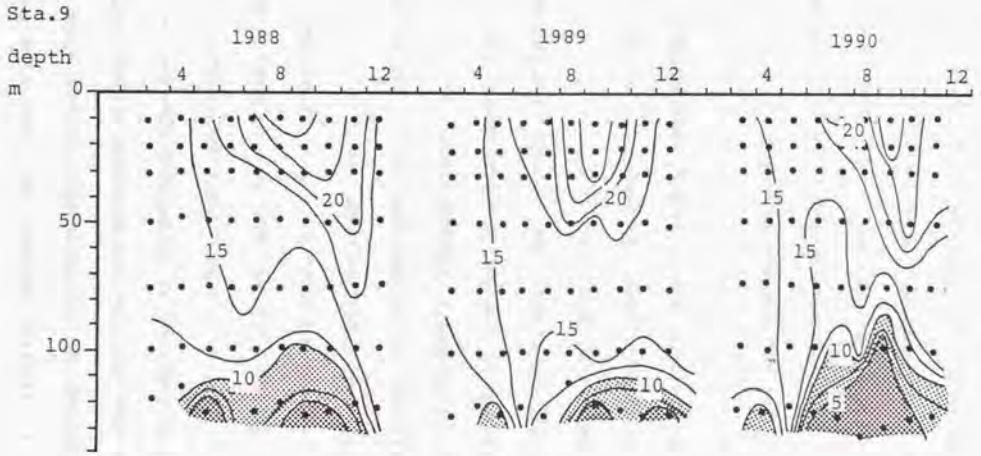

Fig. 26. Temporal variation of the temperature profile (in °C) at Sta.9 in the Western Channel (see Fig. 3 for its position) from 1988 to 1990. The domain where the temperature is lower than 10 °C is shaded and that lower than 5 °C is shaded heavily.

summer-autumn 1990. This suggests that the process of the baroclinic adjustment following the intrusion of the bottom cold water discussed in Section 3 plays an important role in lowering the sea level at the Korean coast.

It should be noted that the intrusion of the bottom cold water in the Western Channel is a local phenomenon, and does not reach the East China Sea (Lim and Chang, 1969). The baroclinic component of the surface current may have a small horizontal scale, and may depend on the selected position of the cross-section.

In the Eastern Channel, almost simultaneous CTD observations were carried out along two observation lines in summer-autumn (October 1988, July 1989 and July 1990) by the Japan Meteorological Agency (JMA, 1990-1992). The positions of the lines are shown with A-A' and B-B' in the uppermost figure in Fig. 27. The cross-sectional temperature distributions are shown in Fig. 27 for each observation: The distributions along A-A' are shown in the upper row and those along B-B' in the lower row. The observations in October 1988 are shown in the left column, those on July 1989 in the central column, and those in July 1990 in the right column.

The seasonal thermocline is well developed in these cross-section, and the isotherms tend to slope down toward the right in each cross section, suggesting that the dominant baroclinic flow is northeastward. The largest contrast in the temperature structure between two sections is seen in the lower layer near the Japanese coast for each observation time. There, the

isotherms run nearly vertical in A-A' line, while the tilting of the isotherms is not so large in B-B'. The associated baroclinic current would be much stronger in A-A' section than in B-B' section. This also indicates that the baroclinic component of the current is very changeable place by place. Although we focused our discussion on the cross-strait structures in this study, the more elaborate three-dimensional analysis would be needed to evaluate the influences of the baroclinic currents on the sea level distribution around the Tsushima Strait.

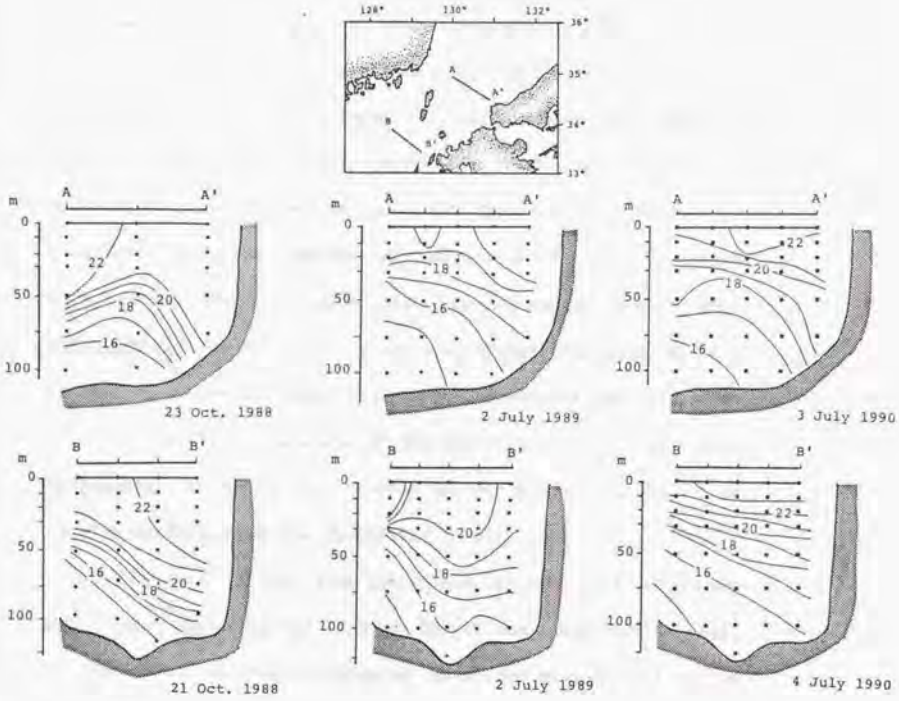

Fig.27. Cross-sectional temperature distributions along line A-A'(the upper figures) and along line B-B' (the lower figures) in October 1988 (the left column), in July 1989 (the central column), and in July 1990 (the right column) when almost simultaneous CTD observations were carried out both of these observation lines. See the uppermost figure for the positions of A-A' and B-B'. The date of the observation is shown below each figure. Note that these observations were made in summer-autumn when the seasonal thermocline was well developed.

5. CONCLUSIONS

The seasonal variation of the volume transport of the Tsushima Warm Current in the Tsushima Strait has been investigated by using both sea level difference data and hydrographic data. According to the former investigations based on the sea level difference or the geostrophic calculation assuming no current near the bottom, the volume transport and the surface current velocity of the Tsushima Warm Current show a remarkable seasonal variation with large amplitude of about 2 Sv. It was also argued that the maximum transport occurs in summer-autumn. By considering the influence of the baroclinic component of the currents on the sea level difference, we showed that these arguments are not correct. The results in this study are summarized below:

(1) ADCP data indicate that the intense current is found even near the bottom in the Tsushima Strait throughout the year. The dynamical calculation assuming no motion near the bottom is not valid to estimate the volume transport through the Tsushima Strait.

(2) The observed sea level difference across the Tsushima Strait contains the influence of the baroclinic current field. To obtain an index for the volume transport and its variation, we need to evaluate the baroclinic sea level difference induced by baroclinic currents, and to subtract it from the observed sea level difference.

(3) It has shown that the baroclinic current structure,

especially in the Western Channel, corresponds to the existence of the bottom cold water in the Tsushima Strait. bottom cold water seems to influence the configuration of the seasonal thermocline and the current structure even in the Eastern Channel.

(4) The analysis of the CTD data being combined with the observed sea level difference data indicates that the total volume transport through the Tsushima Strait has a maximum in early winter and a minimum in early spring. The variation range of the volume transport through the Strait is estimated to be about 0.7 Sv. This value is from 1/3 to 1/2 of the variation deduced from the observed sea level difference where the effect of the baroclinic sea level difference is ignored.

(5) The volume transport through the Western Channel, however, shows the variation similar to the observed sea level variation, though its magnitude is significantly reduced. The maximum transport occurs in September-October, and the minimum transport in March-April. The volume transport through the Eastern Channel is high in November-April, and low in July-October, showing rather negative correlation to the variation through the Western Channel.

(6) The baroclinic current structure is suggested to have a relatively small horizontal scale (and so small time scale), and to depend on the position of selected cross-section.

(7) The total volume transport through the Tsushima Strait estimated by a snap-shot type ADCP observation indicates rather

large seasonal variation of order of 5 Sv. We think this is the overestimation as the error is arisen from temporary shorter fluctuations, from possible wind drift and so on. Surveys throughout the year show that the volume transport is around 1-6 Sv.

ACKNOWLEDGMENTS

The author would like to express his sincere thanks to Prof. T. Yanagi of the Ehime University, the late Prof. S. Tawara of the Shimonoseki University of Fisheries and Prof. Y. Nagata of the University of Tokyo for their discussions, suggestions and encouragements. He also expresses many thanks to Prof. A. Kaneko of Hiroshima University and Dr. H. Takeoka, Dr. Y. Isoda, Mr. H. Akiyama of the Ehime University for their fruitful discussions. The author is much indebted to the Japan Oceanographic Data Center and Mr. M. Kawano of the Yamaguchi Prefectural Open-Sea Fisheries Experimental Station for kindly supplying the necessary data. Thanks are also due to Capt. Okuda, the officers and crews of R.V. Kuroshio-Maru, the Yamaguchi Prefectural Open-Sea Fisheries Experimental Station for their heartily supports during the observations. Finally, he would like to note that this work would not be complete without encouragements of his wife and daughter.

REFERENCE

Bowden,K.F. and A.P.Fairbrain(1952):A determination of the frictional forces in a tidal current. Proceedings of the Royal Society, London, **A214**, 371-392.

Byun,S.K. and Y.H.Seung(1984):Description of current structure and coastal upwelling in the southwest Japan Sea - summer 1981 and spring 1982. In:Ocean Hydrodynamics of the Japan and East China Seas, ed. by T.Ichiye, Elsevier, Amsterdam, 83-93.

Byun,S.K.(1989):Sea surface cold water near the southern coast of Korea: wind effect. The Journal of Oceanological Society of Korea, **24**, 121-131.

Egawa,T., Y.Nagata and S.Sato(1993):Seasonal variation of the current in the Tsushima Strait deduced from ADCP data of ship-of-opportunity. Journal of Oceanography, **49**, 39-50.

Hidaka,K. and T.Suzuki(1950):Secular variation of the Tsushima Current. Journal of the Oceanographic Society of Japan, **16**,28-31(in Japanese).

Isoda,Y.(1989):Topographic effect of the Tsushima Island on the Tsushima Warm Current. Bulletin on Coastal Oceanography, **27**, 76-84(in Japanese).

Japan Meteorological Agency(1990,1991,1992):The Results of the oceanographical observations, **82**.

Japan Oceanographic Data Center(1985):JODC catalog, **16**.

Kajiura,K.,M.Tsuchiya and K.Hidaka(1958):The analysis of oceanographical condition in the Japan Sea. Report of the Development of the Fishries Resources in the Tsushima Warm

Current, 1, 158-170(in Japanese).

Kaneko,A.,Y.Hashimoto,M.Ishibashi and A.Tasiro(1988): Acoustic Doppler Current Profiler. Bulletin of Research Institute for Applied Mechanics, 66, 47-76(in Japanese).

Kaneko,A.,W.Koterayama,H.Honji,S.Mizuno,K.Kawatate and R.L.Gordon (1990):Cross-stream survey of the upper 400 m of the Kuroshio by an ADCP on a towed fish. Deep Sea Research, 37, 875-889.

Kawabe,M.(1982):Branching of the Tsushima Current in the Japan Sea,Part I. Data analysis. Journal of the Oceanographic Society of Japan, 38, 95-107.

Lim,D.B. and S.D.Chang(1969):On the cold water mass in the Korea Strait. Journal of the Oceanological Society of Korea, 4, 71-82.

Lim,D.B.(1971):On the origin of the Tsushima Current water. Journal of the Oceanological Society of Korea, 6, 85-91.

Miita,T.(1976):Current characteristics measured with current meter at the fixed station. Bulletin of the Japanese Society of Fisheries Oceanography, 28, 33-58(in Japanese).

Mizuno,s., K.Kawatate, T.Nagahama and T.Miita(1989):Measurements of East Tsushima Current in winter and estimation of its seasonal variability. Journal of the Oceanographic Society of Japan, 45, 375-384.

Nagata,Y.(1982):Oceanic conditions in the East China Sea. Proceedings of the Japan-China Ocean Study Symposium October 28-29, 1981, Special Report of Institute of Oceanic Research Tokai University.

National Fisheries Research and Development Agency of

Korea(1992):Annual Report of Oceanographic Observations, **35**.

Odamaki,M.(1989):Tides and tidal current in the Tsushima Strait. Journal of the Oceanographic Society of Japan, **45**, 65-82.

Ogawa,Y.(1983):Seasonal changes in temperature and salinity of water flowing into the Japan Sea through the Tsushima Strait. Bulletin of the Japanese Society of the Fisheries Oceanography, **43**, 1-8(in Japanese).

Shikama,N.,T.Saito,T.Iwao,N.Kubo,M.Fujiwara and T.Nakagawa(1991): The current measurements in the Tsugaru Strait using bottom installed ADCP(III). Abstracts of papers, Autumn Meeting of Oceanographic Society of Japan, 173(in Japanese).

Simpson,J.H., E.G.Mitchelson-Jacob and A.E.Hill(1990):Flow structure in a channel from an acoustic Doppler current profiler. Continental Shelf Research, **10**, 589-603.

Tawara,S. T.Miita and T.Fujiwara(1984):The hydrography and variability in the Tsushima Straits. Bulletin on Coastal Oceanography, **22**, 50-58(in Japanese).

Tawara,S. and T.Fujiwara(1985) Sea surface temperature distribution and its variability across the Tsushima Strait. Journal of the Oceanographic Society of Japan, **41**, 49-55.

Toba,Y., K.Tomizawa, Y.Kurasawa and K.Hanawa(1982):Seasonal and year-to-year variability of the Tsushima-Tsugaru Warm Current system with its possible cause. La Mer, **20**, 41-51.

Uda,M.(1934):The results of simultaneous oceanographical investigations in the Japan Sea and its adjacent waters in May and June, 1932. Journal of the Imperial Fisheries Experimental Station, **5**, 57-190(in Japanese).

Uda,M.(1936):Results of simultaneous oceanographical investigations in the Japan Sea and its adjacent waters during October and November, 1933. Journal of the Imperial Fisheries Experimental Station, 5, 57-190(in Japanese).

Yanagi,T. and A.Higuchi(1980):Tide and tidal current in the eastern part of the Seto Inland Sea, Bulletin on Coastal Oceanography, 17, 7-12(in Japanese).

Yi,S.U.(1966):Seasonal and secular variations of the water volume transport across the Korea Strait. Journal of the Oceanological Society of Korea, 1, 7-13.

LIST OF FIGURES

the predicted tidal current at each time of the ADCP observation. The uppermost figure shows the position, where the tidal current component is predicted, relative to the ADCP observation line. The attached Sta. numbers indicate the positions of the CTD observations. The positions are located very near to the line, and we assumed that the positions are aligned on the line. The dates attached to the each figure indicate the starting time and terminating time of the coverage of the ADCP observation line. The northeastward current is taken to be positive.

Fig. 5. Coss-sectional distributions of water temperature in °C. The depth in m is taken in the ordinate, and the scale of the horizontal axis is shown in the right-bottom of each figure. The positions of the CTD stations are shown above each figure. The date of the observation is shown below each figure(a-e).

Fig. 6. Cross-sectional distributions of salinity.

Fig. 7. Cross-sectional distributions of sigma-t.

Fig. 8. Horizontal velocity field obtained by ADCP observations. The velocities are shown in vectors by taking the northward component upward, and the east component rightward. The magnitude of the vector is shown at the bottom of each figure. The tidal current correction has not

been made. The date of the observation is shown below in each figure.

Fig. 9. Distributions of the northeastward component of the current velocity in cm/sec. The northeastward direction is perpendicular to the section and coincides roughly with the strait axis. The tidal correction (see Section 2-2) has been made, and the values are smoothed by taking average for each 16m x 10 km rectangular area. The date of the observation is shown below each figure. The domains where the current is southwestward are shaded.

Fig. 10. Temporal and spatial variations in the volume transport. The volume transport is defined as the vertically integrated current at each point, here. They are the total values for each 10 km segment. The ADCP data is not available near the bottom, and we used three kind of assumption to fill the current profile in the shadow zone: no current in the shadow zone is assumed in case 1 (the upper left figure), a linear profile vanishing at the bottom in case 2 (the upper right figure), and a quadratic profile in case 3 (the lower figure). See the text for details. The shaded region indicates southward volume transport.

Fig. 11. The total volume transports in Sv (the integrated transport over the whole section) for four observation times. The integration does not made for the data on

October 31, as the data are not available in the Western Channel where the strong current zone of the Tsushima Warm Current flows. Open circles denote the estimations for Case 1, and the closed circles for Case 2, the open triangles for the Case 3.

Fig. 12. Wind in the Beaufort's scale measured on the ship during observations.

Fig. 13. The same as in Fig. 9, except for the northeastward component of the baroclinic flow in cm/sec: (a) in September 1990 and (b) in March 1991. The former is conseidered as a representative for summer-autumn contdition, and the latter for winter-spring. The shaded area indicates southwestward flow.

Fig. 14. Horizontal distributions of the temperature in °C in the bottom layer of the Western Channel in August 1963 (the left figure) and in November 1966 (the right figure). (after Lim and Chang,1969)

Fig. 15. Horizontal distribution of the temperature in the bottom layer of the Western Channel in August 1990.

Fig. 16. Skematic view of the models and the initial shape of the upper boundary of the bottom cold water used in this study: (a) Model 1, and (b) Model 3. The stratification in Model 2 is the same as Model 3, but the initial position of the bottom

cold water is the same as in Model 1. See the text for details.

Fig. 17. The shapes of the surface/interface elevation (full line: see the left ordinate for its scale) and of the northeastward component of the velocity parpendiculer to the section (broken line: see the right ordinate for its scale) after a qusi-steady state is achieved: (a) for the Model 1, (b) Model 2 and (c) Model 3. Note that the vertical scale for the displacement is changed figure by figure.

Fig. 18. The temporal variations of the differences in daily mean sea level between Izuhara and Pusan (the upper figure) and between Hakata and Izuhara (the lower figure) from 1988 to 1990. The broken line shows the 30-day running mean. The differences are obtained by subtracting the value at Pusan from that at Izuhara for the upper figure, and the value at Izuhara from that at Hakata for the lower figure. The zero line corresponds the averaged sea level difference in the analyzed period.

Fig. 19. Coss-sectional distributions of water temperature (a: in °C), salinity (b) and sigma-t (c). The depth in m is taken in the ordinate. The positions of the CTD stations are shown above each figure. The date of the observation is shown below each figure.

Fig. 20. Model used to calculate the baroclinic current profile (dotted line), the baroclinic surface speed (V_o) and the sea level gradient $\Delta\eta$, between the neiboring satations A and B. See the text for details.

Fig. 21. The temporal and spatial variation of the baroclinic sea level. The sea level is plotted relative to that at the Japanese coast. The contour interval is 1 cm. The shaded area indicates the domain where the sea level lower than -5 cm.

Fig. 22. Temporal variations of the sea level difference (in cm) across the Western Channel (the upper figure) and across the Eastern Channel (the lower figure). The baroclinic sea level difference is shown with a black circle, and the observed sea level difference (30-day running mean) with a open circle. The data for the observed sea level difference are shown only when the baroclinic sea level difference data are available.

Fig. 23. The same as in Fig. 22, except fot the barotropic sea level differences.

Fig. 24. Seasonal variations of the observed sea level differences (the left culumn), the baroclinic sea level difference (the central column) and the barotropic sea level difference (the right column) across the Western Channel (the upper figure) and across the Eastern Channel (the

lower figure).

Fig. 25. Seasonal variation of the barotropic sea level difference (in cm, see the left ordinate: the solid line) across the whole Tsushima Strait. The corresponding value of the transport in Sv is taken along the right ordinate. The observed sea level difference (in cm, see the left coordinate: dash-dotted line) across the strait and the bottom-referred geostrophic transport (in Sv, see the right coordinate: dashed line) obtained from the density distribution shown in Fig. 19, are also shown in the figure.

Fig. 26. Temporal variation of the temperature profile (in °C) at Sta.9 in the Western Channel (see Fig. 3 for its position) from 1988 to 1990. The domain where the temperature is lower than 10 °C is shaded and that lower than 5 °C is shaded heavily.

Fig. 27. Cross-sectional temperature distributions along line A-A'(the upper figures) and along line B-B' (the lower figures) in October 1988 (the left column), in July 1989 (the central column), and in July 1990 (the right column) when almost simultaneous CTD observations were carried out both of these observation lines. See the uppermost figure for the positions of A-A' and B-B'. The date of the observation is shown below each figure. Note that these observations were made in summer-autumn when the seasonal

thermocline was well developed.

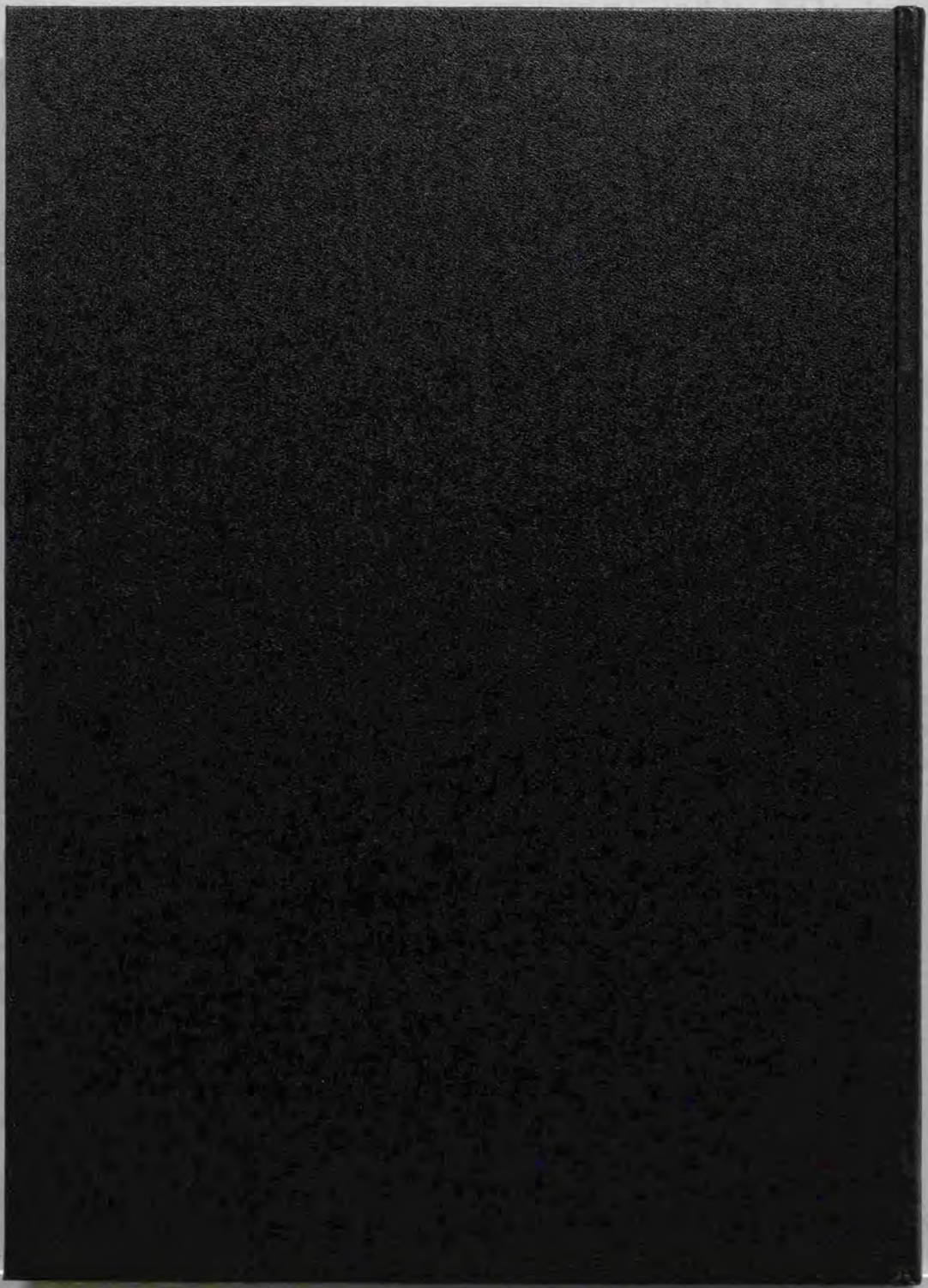

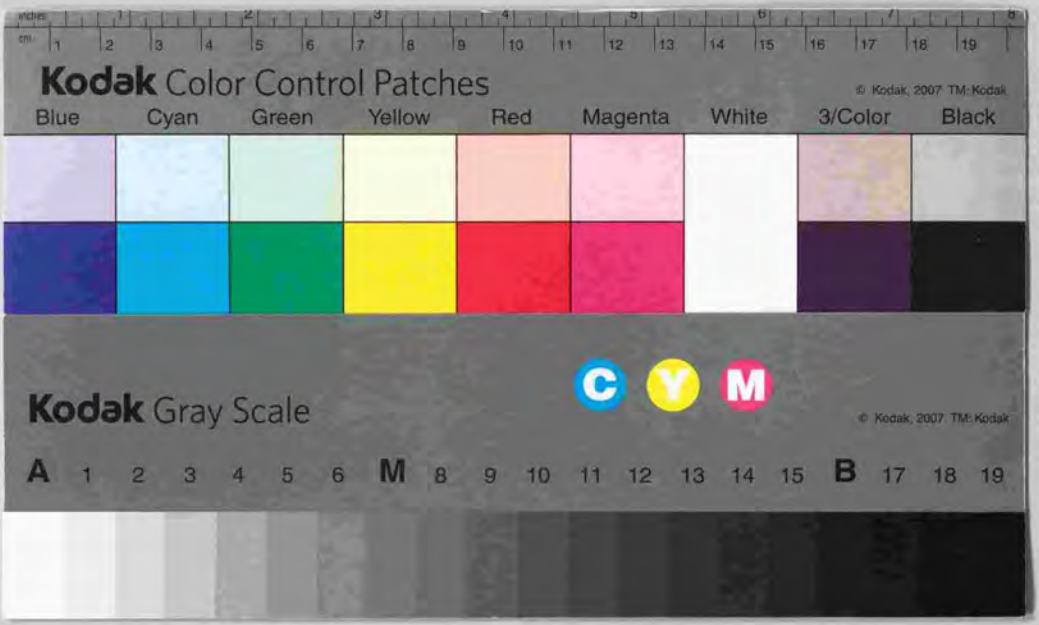
inches
cm
Kodak Color Control Patches
© Kodak, 2007 TM: Kodak
Blue
Cyan
Green
Yellow
Red
Magenta
White
3/Color
Black
Kodak Gray Scale
C
Y
M
© Kodak, 2007 TM: Kodak
A 1 2 3 4 5 6 M 8 9 10 11 12 13 14 15 B 17 18 19